CHEMISTRY OF MATERIALS

pubs.acs.org/cm

Article

Magnetic Metal Micelles for Enhanced Delivery of Self-Immolating CD8$^+$ T-Cell Epitopes for Cancer Immunotherapy

Jiexin Li, He Ren, Yaping Sun, Gengqi Liu, Xingyue Yang, Qian Qiu, Yuanmeng Ding, Jonathan F. Lovell, and Yumiao Zhang*

Cite This: *Chem. Mater.* 2021, 33, 9780−9794

Read Online

ACCESS | Metrics & More | Article Recommendations | Supporting Information

ABSTRACT: Cancer peptide vaccines face challenges for antigen delivery and presentation. In the present work, we develop a self-assembled magnetic micelle delivery system for CD8$^+$ T-cell epitopes that produces strong cellular immune responses. Hydrophobically modified imiquimod R837 and $Zn_{1.15}Fe_{1.85}O_4$ are coencapsulated in the core of Pluronic F127 block copolymer micelles. Magnetic $Zn_{1.15}Fe_{1.85}O_4$ enables externally targeted delivery and enrichment of micelles in lymph nodes. Furthermore, metal ions are found to enhance vaccine immunogenicity. F127 micelles were chemically modified by a self-immolative linker so that antigens are rapidly and reversibly grafted on micelles in an aqueous solution. With the assistance of an external magnetic field, once the magnetic micelles are delivered to lymph nodes and taken up by immune cells, intracellular glutathione cleaves the disulfide bond and releases pristine short peptide antigen. Delivery to lymph nodes is tracked by magnetic resonance and fluorescence imaging. The use of this vaccine system eradicated tumors in a murine tumor model. Thus, integrating multiple functionalities in a single micellar delivery system, including responsive linkage, multiple immunostimulatory molecules, targeted delivery, and bimodal imaging, demonstrates the potential for theranostic approaches to develop a new generation of cancer vaccines.

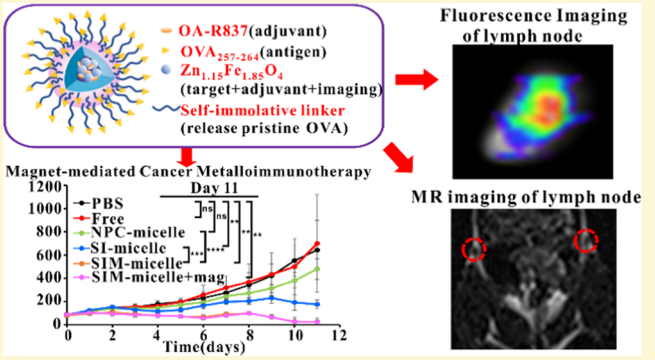

1. INTRODUCTION

Immunotherapy regulates the immune system and has attracted extensive attention for cancer treatment, but clinical results leave room for improvement.[1−4] Many challenges have impeded the development of immunotherapy, including the inability to produce sufficient antigen-specific CD8$^+$ T cells, an immunosuppressive tumor microenvironment, and difficulties for T cells to reach and engage tumor cells. Cancer vaccines may have nonoptimal codelivery of antigens and adjuvants to immune cells in draining lymph nodes (dLNs). As various vaccine systems have been developed, some ongoing endeavors focus on the induction of sufficient cross-presentation and dendritic cell (DC) activation to trigger the dendritic cell-derived costimulatory factors, presenting key steps to initiate an effector CD8$^+$ T-cell response.[5−7] Toward that end, several vaccine preparation methods have been designed for the incorporation of antigens and adjuvants to the nanovaccine, including encapsulation in nanoparticles or adsorbing on the surface *via* electrostatic interactions.[8] However, due to the hydrophilic cargo, low encapsulation rate and poor stability lead to premature release and fast clearance after circulation.[9−11] Alternatively, covalently binding methods have been adopted for the conjugation to liposomes and other carriers.[12,13] However, the covalent linkage leads to reduced immunogenicity without releasing the pristine antigens in DCs, resulting from the impaired interaction between the antigen peptide and the major histocompatibility complex (MHC) molecule.[14,15] Noncovalent binding strategies suffer from limitations such as instability in physiological condition media,[16,17] although some new vaccine formulations such as the cobalt−porphyrin liposomal vaccine systems can solve this problem by generating strong cellular immune responses for the treatment of malaria, cancers, and others.[18−20]

Activation of CD8$^+$ T cells requires a series of processes, including antigen presentation and activation of costimulatory molecules. The Hubbell group introduced self-immolative linker-based vaccines for enhanced immunotherapy that can responsively and reversibly release pristine antigens in DCs but stability was well maintained before delivery to dLNs.[21] Compared to self-immolative linkers, the non-self-immolative cross-linker (such as Traut's reagent) could only release tagged

Received: October 25, 2021
Revised: November 23, 2021
Published: December 10, 2021

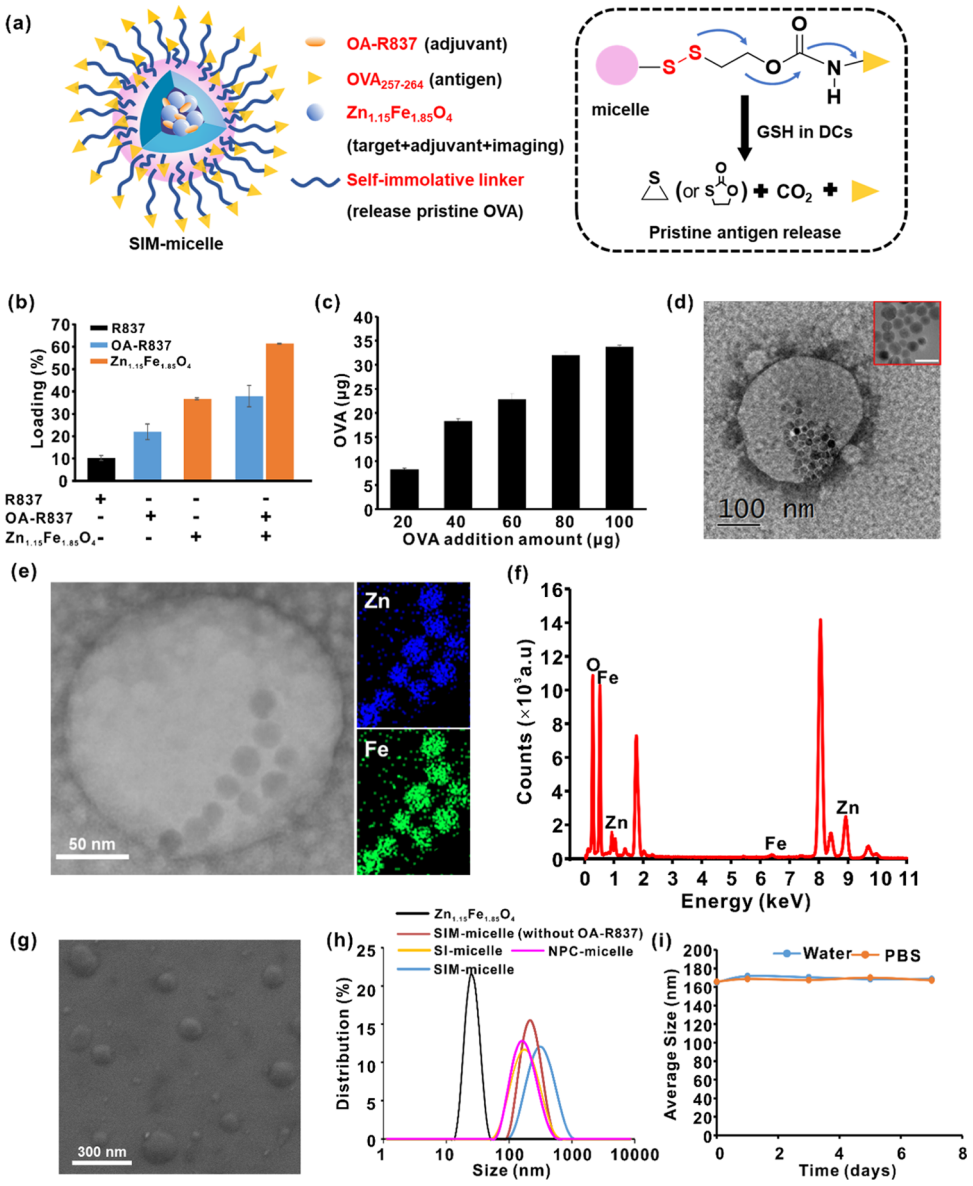

Figure 1. Preparation and characterization of SIM-micelles. (a) Schematic illustration of the preparation of SIM-micelles. After the OA-R837 adjuvant and small $Zn_{1.15}Fe_{1.85}O_4$ nanoparticles were self-assembled into magnetic micelles of SI-F127, the $OVA_{257-264}$ model antigen was readily grafted on SIM-micelles *via* a GSH-responsive self-immolative linker in aqueous solution, forming self-immolative magnetic micelles ("SIM-micelles"). (b) Coloading effect of $Zn_{1.15}Fe_{1.85}O_4$ and OA-R837 (n = 3; mean ± standard deviation (SD)). (c) Different amounts of $OVA_{257-264}$ were grafted on micelles (n = 3; mean ± SD). (d) Transmission electron microscopy (TEM) of SIM-micelles, scale bar: 100 nm. (The inset image framed in red is $Zn_{1.15}Fe_{1.85}O_4$, scale bar: 40 nm.) (e) Energy-dispersive X-ray (EDX)-mapping images and (f) energy-dispersive spectrometry (EDS) image of SIM-micelles. (g) Scanning electron microscopy (SEM) image of SIM-micelles. (h) Size distribution of aqueous SIM-micelles and controls, including SI-micelles, *p*-nitrophenyl chloroformate (NPC)-micelles, SIM-micelles (but without the encapsulation of OA-R837), and $Zn_{1.15}Fe_{1.85}O_4$ nanocrystals (in tetrahydrofuran (THF)) measured by dynamic light scattering (DLS). (i) Stability of SIM-micelles in an aqueous solution or phosphate-buffered saline (PBS) solution during 1 week of storage at room temperature.

antigen after disulfide reduction, which significantly reduced the immunogenicity of the antigen.[21,22] With respect to the activation of DCs, commonly used adjuvants include imiquimod (R837),[23,24] monophosphoryl lipid A, resiquimod,[25−27] CpG oligonucleotide,[28,29] metals,[30,31] and others. Among them, metal-based adjuvants have shown great promise in metalloimmunotherapy. It has been found that manganese ions and zinc ions could trigger multifaceted type I interferon (IFN)-driven inflammatory responses to activate innate immunity.[32,33] Zn^{2+} involves in the upregulated expression of various toll-like receptors (TLRs) (TLR 1, 2, and 6) and a variety of inflammatory cytokines (such as interleukin (IL)-6, IFN-γ, and tumor necrosis factor (TNF)-α) in macrophages when introduced along with antigen.[34] Although some metal elements have been employed for chemotherapy, metal-loimmunotherapy has recently been proposed as a future direction for cancer treatments.[35−37]

In addition, magnetic metal-based biomaterials such as Fe_3O_4-encapsulated nanovaccines can be mediated to lymph nodes by an external magnetic field exerted for targeting delivery.[38−40] A typical strategy is that magnetic nanovaccines were preingested in dendritic cells (DCs) *in vitro* and then magnetically targeted to dLNs.[38,39] Other adoptive immune cell therapies are not always effective for solid tumor treatment

https://doi.org/10.1021/acs.chemmater.1c03681
Chem. Mater. 2021, 33, 9780−9794

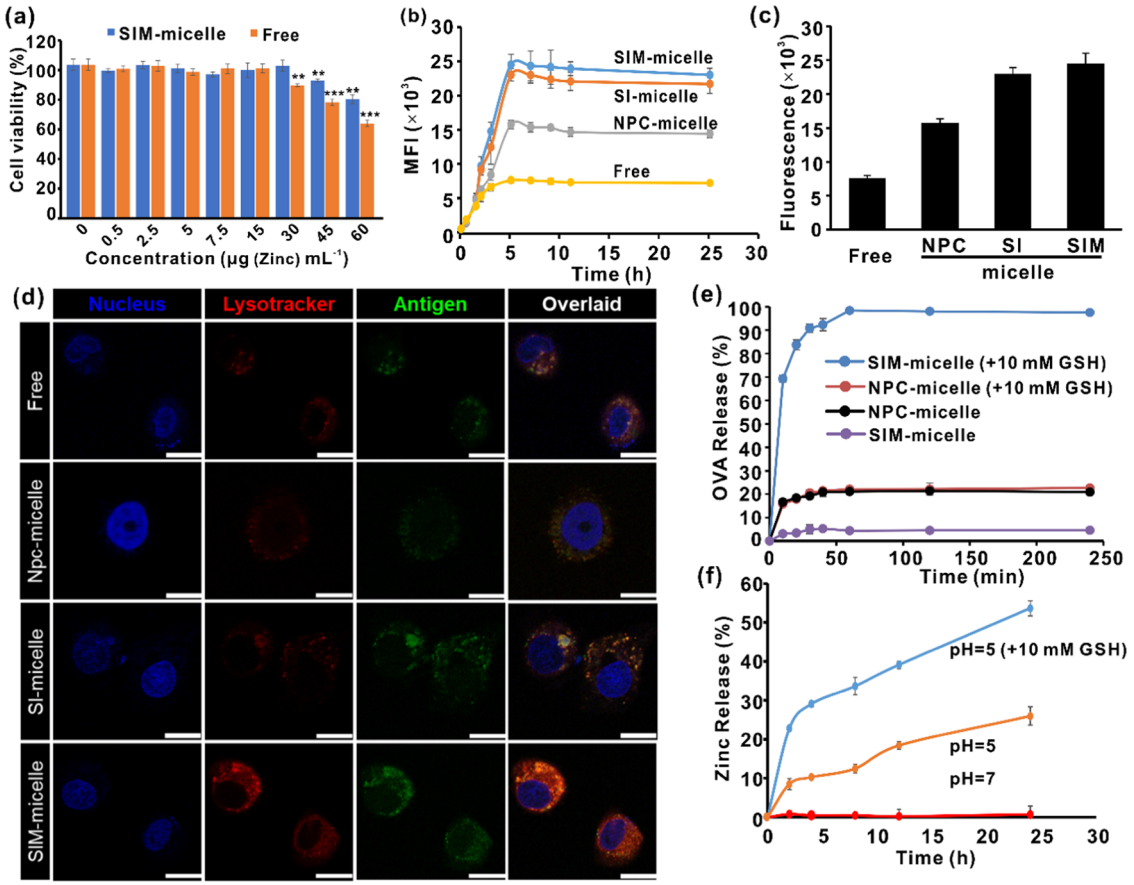

Figure 2. Uptake and release of SIM-micelles *in vitro*. (a) Cell viability of DC2.4 incubated by SIM-micelles and free forms at different concentrations (n = 3; mean ± SD). (b) Uptake kinetics and (c) cellular uptake at 5 h of FITC-labeled SIM-micelles and control formulations by DC2.4 (n = 3; mean ± SD). (d) Confocal microscopic images of DC2.4 cells incubated with FITC-labeled $OVA_{257-264}$ in forms of free, NPC-micelles, SI-micelles, and SIM-micelles. Blue = cell nucleus, red = lysosome, and green = $OVA_{257-264}$; scale bar = 10 μm. (e) Reduction-responsive release of $OVA_{257-264}$ from SIM-micelles and NPC-micelles with or without 10 mM GSH (n = 3; mean ± SD). (f) Zinc release kinetics from SIM-micelles with or without GSH at different pH values. One-way analysis of variance (ANOVA) analysis with two-tailed unpaired Student's t-test was used for significant difference analysis, *P < 0.05, **P < 0.01, ***P < 0.001, and ****P < 0.0001.

and might also cause side effects and cytokine storm due to the off-target effect.[41,42] Furthermore, some metal-based materials with optical and paramagnetic properties can be used as contrast agents to image and track the delivery process of the vaccine.[43] Although the low sensitivity of magnetic resonance (MR) imaging (MRI) using Fe_3O_4 is one concern for the applications of tumor theranostics,[44,45] doping with zinc ions in Fe_3O_4 has been explored to improve the paramagnetism of nanoparticles.[43,46]

Taking the aforementioned points together, we designed a multifunctional magnetic anticancer nanovaccine that can generate an enhanced $CD8^+$ T-cell response for targeting delivery mediated by an external magnetic field. Dual adjuvants, including imiquimod and inorganic $Zn_{1.15}Fe_{1.85}O_4$, were coencapsulated in the Pluronic F127 block copolymer. Antigens were conjugated on the surface micelles by a self-immolative linkage. Once targeted delivery is induced to the DCs in lymph nodes, nanovaccines can responsively and reversibly release pristine antigens, cleaved by the higher concentration of intracellular glutathione (GSH). In addition to endowing the nanovaccine to be paramagnetic for the targeting delivery, $Zn_{1.15}Fe_{1.85}O_4$ could also release zinc ions in the acidic environment in lysosomes that activated the pathways of metalloimmunotherapy. Using these multifunctional hybrid nanoparticles, magnetically targeted delivery to lymph nodes could be achieved and tracked by magnetic resonance imaging. Importantly, significantly enhanced antigen presentation and dendritic cell maturation were induced. Also, high antitumor efficacy with a 100% survival rate and no recurrences was demonstrated in a murine tumor model.

2. RESULTS AND DISCUSSION

2.1. Synthesis and Characterization of Self-Immolative Magnetic (SIM)-Micelles. To prepare self-assembled magnetic SIM-micelles (Figure 1a), we first grafted a self-immolative linker to Pluronic F127 to form an amine-reactive and self-immolative F127, termed SI-F127. Figures S1 and S2 show the synthetic route and characterization. The adjuvant imiquimod (R837) was encapsulated in SI-F127 micelles by hydrophobic interactions. However, the encapsulation efficiency was only 10.2% (Figure 1b). Therefore, R837 was hydrophobically modified by oleoyl chloride (OA) by a thermal decomposition method at high temperatures, and the resulting OA-modified R837 (OA-R837) was purified by chromatography. Figures S3 and S4 show the synthetic route and characterization. After hydrophobic modification by oleic acid, the fluorescence spectrum peak used for imiquimod quantification was unchanged (Figure S5). The encapsulation of the modified OA-R837 doubled to over 20%, compared to R837 (Figure 1b). Another compound, $Zn_{1.15}Fe_{1.85}O_4$, that can

https://doi.org/10.1021/acs.chemmater.1c03681
Chem. Mater. 2021, 33, 9780−9794

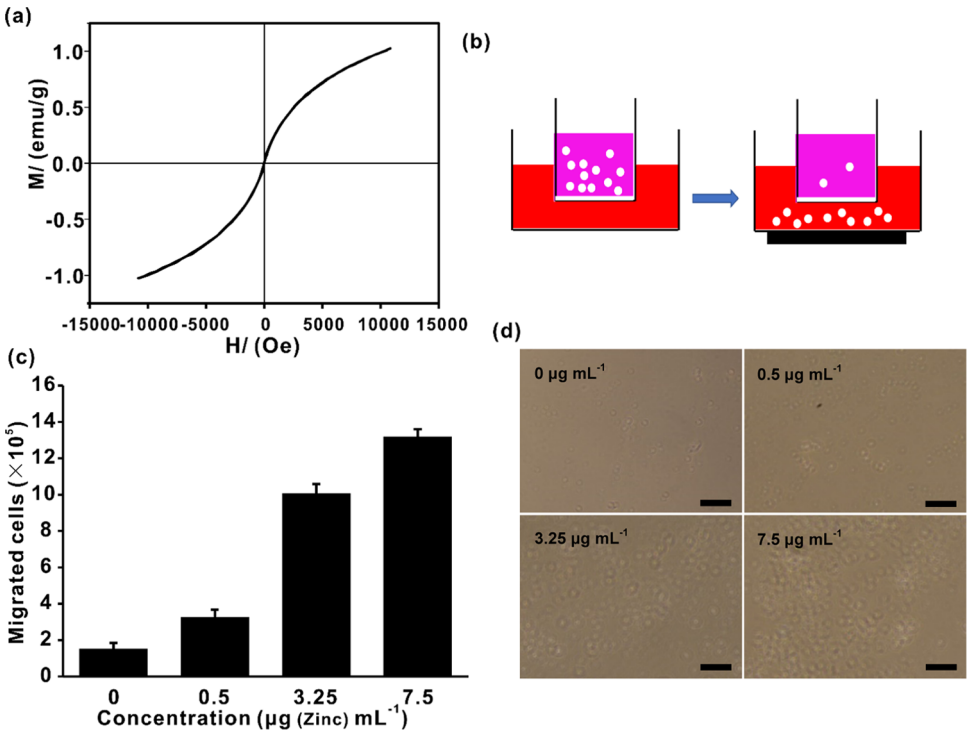

Figure 3. *In vitro* migration of BMDCs uptaking magnetic SIM-micelles in a magnetic field. (a) Magnetic properties of SIM-micelles. (b) Illustration of the transwell experimental setup. Fresh 1640 medium was placed (without fetal bovine serum (FBS)) in the lower chamber, BMDCs with different concentrations of SIM-micelles were resuspended in a cell six-well culture chamber with a magnet attached to the bottom of the chamber for 2 h. (c) Number of migrated cells from the upper to lower chamber counted *via* a hemocytometer mediated by different concentrations of SIM-micelles (n = 3; mean ± SD). (d) Representative images of migrated cells in the low chamber. BMDCs with different concentrations of SIM-micelles were resuspended in a cell six-well culture chamber with a magnet attached to the bottom of the chamber for 2 h, and the photograph of the migrated cells was acquired. Scale bar: 50 μm. The concentration of $Zn_{1.15}Fe_{1.85}O_4$ was characterized by measuring the zinc ions by inductively coupled plasma optical emission spectrometry (ICP-OES).

be used for MR imaging and magnet-mediated targeting delivery was coloaded with OA-R837 in SI-F127 micelles. Remarkably, as shown in Figure 1b, the encapsulation yield of OA-R837 and $Zn_{1.15}Fe_{1.85}O_4$ in micelles synergistically increased to about 38 and 61%, respectively, presumably owing to the coloading of the other.[47,48] Another advantage of SIM-micelles is that amine-containing ovalbumin (OVA) antigen could be easily and rapidly conjugated on the surface of micelles by simply adding OVA in an aqueous solution. As shown in Figure 1c, more OVA was grafted as increasing OVA was added to 1 mL of 9 μg (zinc) mL^{-1} SIM-micelle aqueous solution and the grafting reached saturation when 80 μg OVA was added.

Negatively stained transmission electron microscopic (TEM) images in Figure 1d show the spherical morphology of SIM-micelles with a size of about 180 nm, containing smaller size spheres corresponding to $Zn_{1.15}Fe_{1.85}O_4$ inorganic nanoparticles (inset). Energy-dispersive X-ray (EDX)-mapping and EDS were carried out in Figure 1e,f verified the presence of Zn and Fe elements (Figure 1e,f). Scanning electron microscopic (SEM) images shown in Figure 1g revealed the size and morphology of SIM-micelles, which is consistent with Figure 1d–f. The size of micelles was also characterized by dynamic light scattering (DLS) measurement, showing that the average size of hydrated SIM-micelles and controls including SI-micelles, NPC-micelles, SIM-micelles (but without the encapsulation of OA-R837), and $Zn_{1.15}Fe_{1.85}O_4$ nanoparticles (suspended in THF) were 178, 152, 163, 150, and 25 nm, respectively (Figure 1h). This change in particle size suggests that OA-R837 and $Zn_{1.15}Fe_{1.85}O_4$ were encapsulated in micelles. Within a 7-day storage period in distilled water or PBS at room temperature, the particle size of SIM-micelles did not change significantly, indicating acceptable storage stability (Figure 1i). Refer to Table S1 for a summary of all of the different formulations used in this study.

2.2. Cellular Uptake and Release *In Vitro*. Next, the endocytosis and release of antigens and adjuvants in dendritic cells were investigated. First, the cytotoxicity of SIM-micelles and free forms (both containing 2 μg mL^{-1} OVA, 4.5 μg mL^{-1} OA-R837, and varying concentrations of $Zn_{1.15}Fe_{1.85}O_4$ of 0–60 μg (zinc) mL^{-1}) was evaluated using DC2.4 cells by the cell counting kit-8 (CCK-8) assay. No significant toxicity was observed in the concentration range of 0–45 μg (zinc) mL^{-1} (Figure 2a) for DC2.4 cells, so safe doses of 7.5 μg (zinc) mL^{-1}, 2 μg mL^{-1} OVA, and 4.5 μg mL^{-1} OA-R837 were used in subsequent *in vitro* experiments. In addition, to demonstrate the self-immolative linkage and traceless release of antigen from SIM-micelles (Figure 1a), we also designed a control, termed *p*-nitrophenyl chloroformate (NPC)-micelles where antigens could still readily be conjugated on the surface of NPC-F127, but *via* a non-self-immolative linkage of NPC. The synthetic route is shown in Figure S1. Antigen-presenting cells, DC2.4, were used to study the interaction with different vaccine formulations, including free form (free OVA + free OA-R837 + $Zn_{1.15}Fe_{1.85}O_4$), SI-micelles (SIM-micelles without magnetic $Zn_{1.15}Fe_{1.85}O_4$ encapsulated in micelles as control, Figure S6), NPC-micelles (OA-R837 and $Zn_{1.15}Fe_{1.85}O_4$ were coloaded in NPC-F127 micelles with OVA grafted on the

https://doi.org/10.1021/acs.chemmater.1c03681
Chem. Mater. 2021, 33, 9780–9794

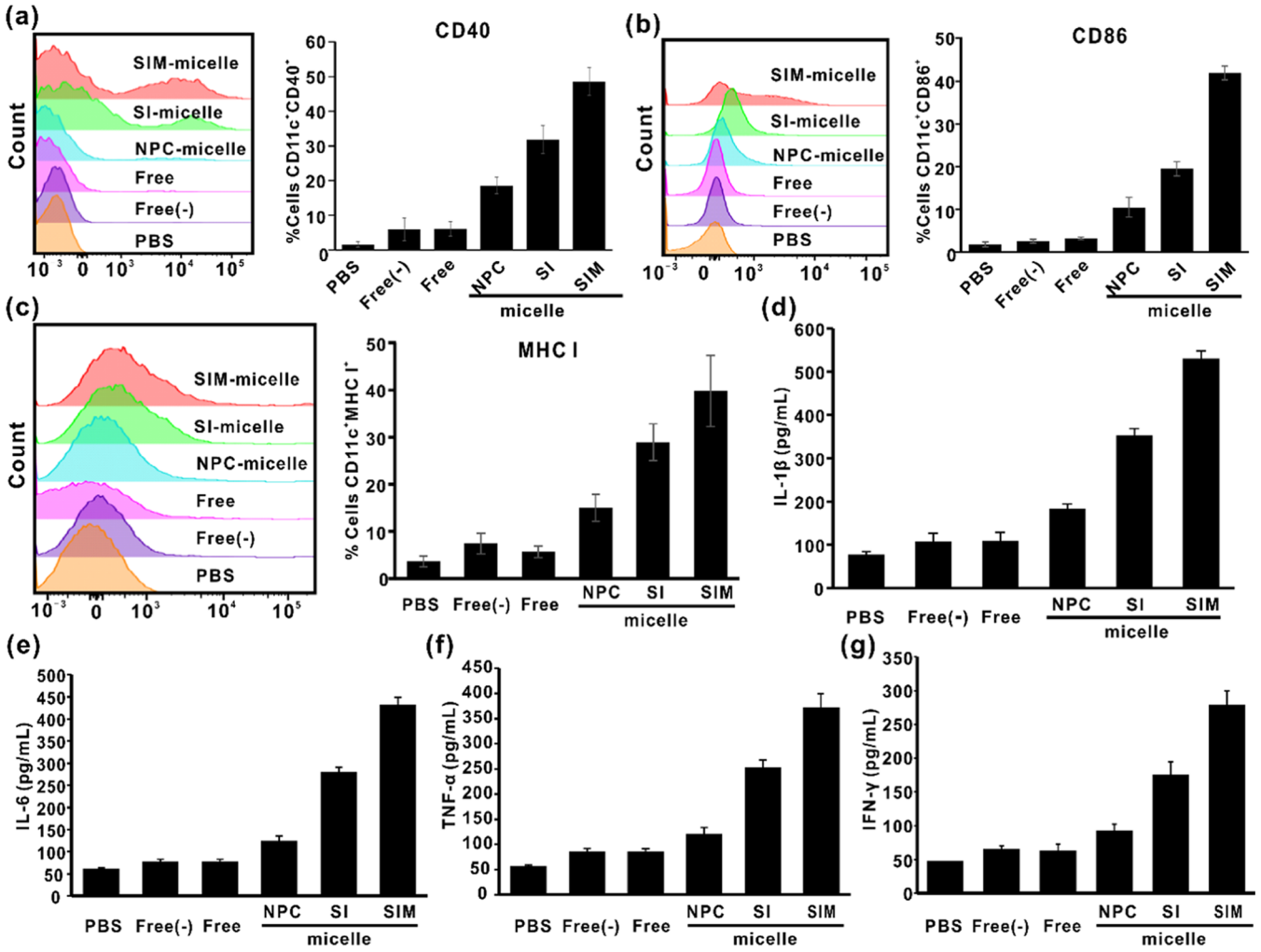

Figure 4. *In vitro* dendritic cell maturation induced by SIM-micelles. Dendritic cells were pulsed with PBS, free (−), free, NPC-micelles, SI-micelles, and SIM-micelles for 48 h. Afterward, the cells were immune-stained with antibodies against CD11c as a dendritic cell marker, and (a) CD40, (b) CD86, or (c) MHC-I as maturation markers were analyzed by flow cytometry. Proinflammatory cytokines, including (d) IL-6, (e) IL-1β, (f) TNF-α, and (g) IFN-γ secreted by DC2.4, were measured after incubation with SIM-micelles or other control formulations (n = 3; mean ± SD). Different vaccine formulations include a free form (free OVA + free OA-R837 + $Zn_{1.15}Fe_{1.85}O_4$), SI-micelles (SIM-micelles without magnetic $Zn_{1.15}Fe_{1.85}O_4$ encapsulated in micelles as a control), NPC-micelles (OA-R837 and $Zn_{1.15}Fe_{1.85}O_4$ were coloaded in NPC-F127 micelles with OVA grafted on the surface), and SIM-micelles (OA-R837 and $Zn_{1.15}Fe_{1.85}O_4$ were coloaded in SI-F127 micelles with OVA grafted on the surface).

surface), and SIM-micelles (OA-R837 and $Zn_{1.15}Fe_{1.85}O_4$ were coloaded in SI-F127 micelles with OVA grafted on the surface). The components of the different formulations are listed in Table S1. OVA was fluorescein isothiocyanate (FITC)-labeled for quantification. Uptake in DC cells could be observed in all of the formulations, reaching saturation after incubation for 5 h (Figure 2b). Since the diameter of SIM-micelles is smaller than 200 nm, SIM-micelles could possibly be ingested *via* the pathways of clathrin-mediated endocytosis, endophilin-mediated endocytosis, or others.[49] Intracellular fluorescence was measured after incubation with vaccines for 24 h followed by cell lysis for analysis. As shown in Figure 2c, the uptake of micellar vaccines by DC2.4 was significantly higher than that of free form. More SIM-micelles and SI-micelles were taken up in cells than NPC-micelles, which might be attributed to higher hydrophobicity of SI-F127 than that of NPC-F127 as previously published results also showed that hydrophobic modification of therapeutic molecules can facilitate their endocytosis.[50−52]

Confocal fluorescence imaging was used to visualize the localization of FITC-labeled $OVA_{257-264}$ in cells. After the DC2.4 cells were incubated with free form antigen, NPC-micelles, SI-micelles, and SIM-micelles for 5 h, it can be clearly seen from Figure 2d that DC2.4 had taken up the most antigen in the SIM-micelle group, overlapping with the lysosomes stained in red. Presumably, pristine antigens were released and the disulfide bond was cleaved following cellular uptake. As shown in Figure 2e, SIM-micelles dialyzed against buffer containing 10 mM GSH could rapidly release 100% pristine OVA with a half-life of several minutes, whereas NPC-micelles could not completely release OVA with or without 10 mM GSH even within 4 h. The pristine OVA could be verified by the same elution time of pristine OVA and released OVA in high-performance liquid chromatography (HPLC) (Figure S8). Furthermore, the release of zinc ions, which can act as an adjuvant for cancer immunotherapy, was also investigated. Since the lysosomal environment features low pH (pH = about 5) and the presence of reducing agents, the $Zn_{1.15}Fe_{1.85}O_4$ decomposition rate and release of zinc were studied in the

https://doi.org/10.1021/acs.chemmater.1c03681
Chem. Mater. 2021, 33, 9780−9794

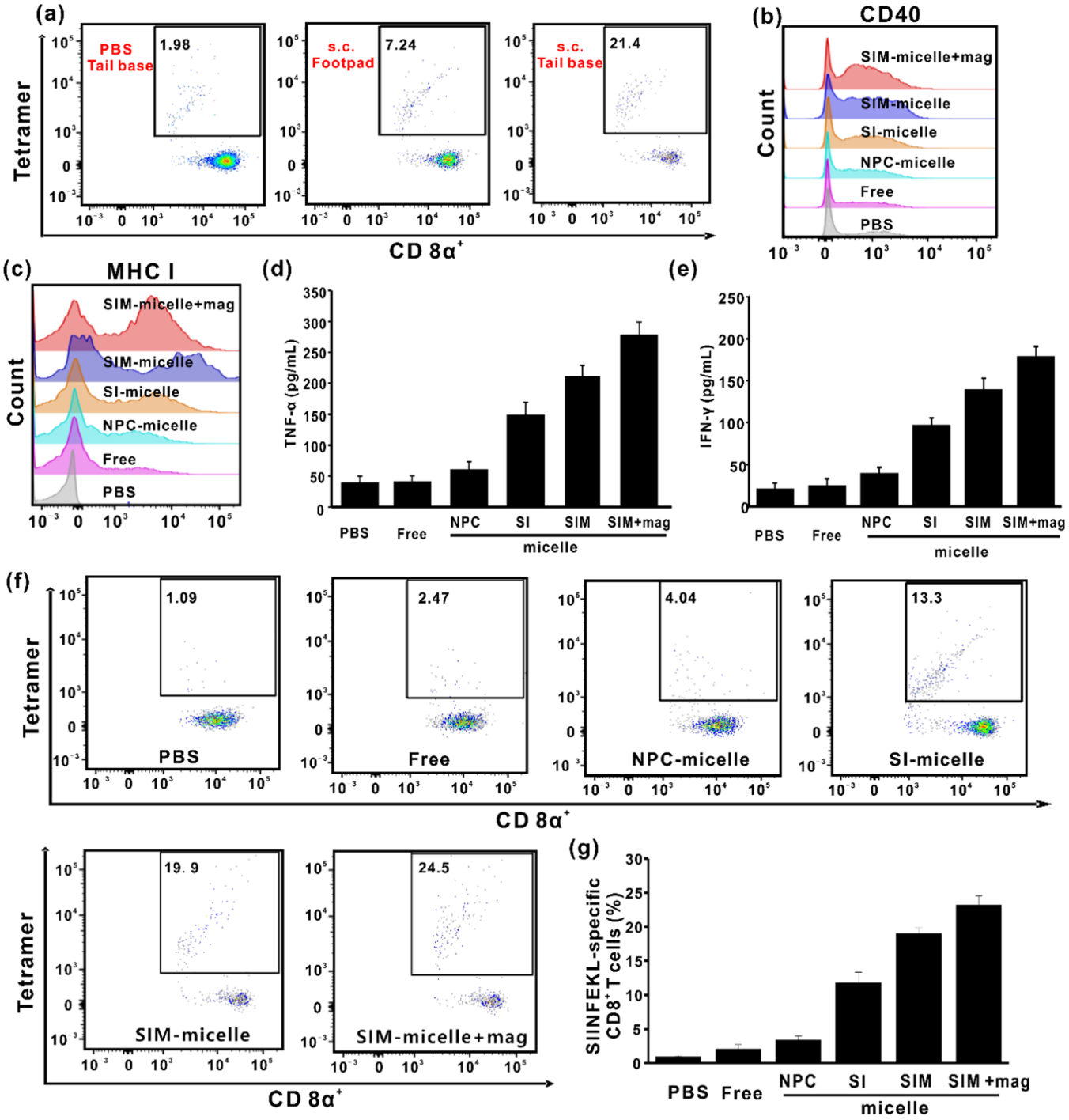

Figure 5. Characterization of *in vivo* T-cell responses. (a) Tetramer staining analysis of T cells specific for $OVA_{257-264}$ by different injection routes. PBS was injected at the tail base as a control, and SIM-micelles were injected at the right footpads or at the tail base. Analysis of the dendritic cell maturation marker (b) CD40 and (c) MHC-I in dLNs after administering SIM-micelles and various control formulations. The concentration of proinflammatory cytokines TNF-α (d) and IFN-γ (e) secreted by immune cells isolated from the peripheral blood serum after vaccination with SIM-micelles or various control formulations (n = 3; mean ± SD). (f) Tetramer staining analysis of T cells specific for $OVA_{257-264}$ after *ex vivo* restimulation of splenocytes from mice vaccinated with SIM-micelles or various controls. (g) Flow-cytometry analysis of the frequency of SIINFEKL-specific $CD8\alpha^+$ T cells in peripheral blood measured 7 days after immunization by SIM-micelles and controls (n = 3; mean ± SD). The following formulations were given to each mouse (amounts of OVA, OA-R837, and $Zn_{1.15}Fe_{1.85}O_4$ in all formulations are all 20 μg for each mouse): free form (free OVA + free OA-R837 + $Zn_{1.15}Fe_{1.85}O_4$), SI-micelles (OA-R837 encapsulated SI-F127 micelles with OVA grafted on the surface but without magnetic $Zn_{1.15}Fe_{1.85}O_4$ encapsulated in micelles), NPC-micelles (OA-R837 and $Zn_{1.15}Fe_{1.85}O_4$ were coloaded in NPC-F127 micelles with OVA grafted on the surface), SIM-micelles (OA-R837 and $Zn_{1.15}Fe_{1.85}O_4$ were coloaded in SI-F127 micelles with OVA grafted on the surface and magnet), and SIM-micelles + mag (SIM-micelles with an external magnetic field).

presence of 10 mM GSH in buffer at a pH of 5 or 7 (Figure 2f). $Zn_{1.15}Fe_{1.85}O_4$ could only be decomposed and released Zn^{2+} at a pH of 5 but not 7. In addition, SIM-micelles released more than 50% Zn^{2+} within 24 h in the presence of 10 mM

https://doi.org/10.1021/acs.chemmater.1c03681
Chem. Mater. 2021, 33, 9780−9794

GSH compared to 20% Zn^{2+} release without GSH, suggesting that SIM-micelles maintain stability in a neutral environment but can release antigens and adjuvants efficiently upon entering DCs. Given the existence of esterase in cells, the degradation of SIM-micelles by esterase was also studied. Thirty-nine percent of Zn^{2+} was released within 24 h in the presence of 1 U esterase compared to 20% Zn^{2+} release without esterase, but the release rate of Zn^{2+} triggered by esterase was slower than that of GSH (Figure S9).

2.3. Magnetically Targeted Delivery *In Vitro*. As the codelivery of antigens and adjuvants to lymph nodes is important for immunogenicity, magnetic $Zn_{1.15}Fe_{1.85}O_4$ was encapsulated in SIM-micelles for magnetically targeted delivery. The magnetic properties of SIM-micelles were first evaluated by field-dependent magnetization ($M-H$). As shown in Figure 3a, after the encapsulation of $Zn_{1.15}Fe_{1.85}O_4$, SIM-micelles became superparamagnetic. This magnetic property was employed to guide the migration of bone marrow-derived dendritic cells (BMDCs) incubated with SIM-micelles using a transwell migration assay (Figure 3b). BMDCs were incubated with different concentrations (0, 0.5, 3.25, 7.5 μg (zinc) mL^{-1}) of SIM-micelles at 37 °C for 5 h, and then the magnetic migration study was carried out in a six-well transwell culture chamber with two layers. BMDCs that ingested SIM-micelles were placed in the upper chamber. After a magnet was placed under a six-well culture chamber for 2 h, the cells migrated into the lower chamber mediated by a magnet. With the increase in the concentration of $Zn_{1.15}Fe_{1.85}O_4$, more cells were collected. When the zinc concentration reached 7.5 μg mL^{-1}, the number of migrated cells was 8.8 times that in the control group where no $Zn_{1.15}Fe_{1.85}O_4$ was used (Figure 3c,d).

2.4. Dendritic Cell Maturation Induced by SIM-Micelles *in Vitro*. Next, the maturation of dendritic cells and the antigen presentation were evaluated *in vitro*. The upregulated expression of costimulatory markers, including CD40, CD86, and MHC-I, were measured by flow cytometry. R837, as a mature toll-like receptor 7 agonist, can significantly stimulate DCs. To show that the hydrophobically modified OA-R837 did not affect the adjuvant effect, we included free and free (−) control groups for comparison, which were formulated with free OVA + free OA-R837 + $Zn_{1.15}Fe_{1.85}O_4$ and free OVA + free R837 + $Zn_{1.15}Fe_{1.85}O_4$, respectively. After incubation with DC2.4 cells separately, there was no significant difference between these two groups with respect to the induction of dendritic cell maturation that was characterized by the expression of maturation markers and cytokines, indicating that OA-R837 modified with oleic acid did not affect its adjuvant effect (Figure 4a−g). Other micellar formulations are the same as in Figure 2. It was also found that the upregulated expression of CD40 and CD86 and the secretion of cytokines such as TNF-α and IFN-γ induced by the SIM-micelle group were significantly higher than those in the SI-micelle group. This showed that $Zn_{1.15}Fe_{1.85}O_4$ had immunostimulatory properties that could further induce the maturation of dendritic cells. As previously reported, the uptake of Zn^{2+} can significantly increase the expression of TLR 1 and downstream signaling molecules of MyD88 and TNFR-related factor 6 in macrophages.[53−55] The enhanced expression of these molecules further activates nuclear factor κB (NF-κB) signaling, inducing the secretion of proinflammatory cytokines and the activation of innate phagocytes. After the uptake by DCs, SIM-micelles dissociated and decomposed in the lysosomal GSH condition, releasing zinc ions that enhanced immunogenicity. In addition, SIM-micelles and SI-micelles induced significantly more dendritic cell maturation and antigen presentation than the NPC-micelle group (Figure 4a−g), owing to the significantly more cellular uptake of SIM-micelles and SI-micelles than that of NPC-micelles (Figure 2a), and also owing to the rapid release of the pristine antigen after self-immolation of the linker (Figures 1a and 2e).

2.5. T-Cell Responses *In Vivo*. Encouraged by these *in vitro* results, we next studied the *in vivo* maturation of dendritic cells and the generation of CD8α^+ T cells to trigger antigen-specific immune responses. First, different SIM-micelle vaccination sites from the tail base or footpad of C57BL/6 mice were compared by analyzing the frequency of SIINFEKL MHC-I tetramer$^+$ CD8α^+ T cells in peripheral blood. Flow cytometry analysis showed that the frequency of SIINFEKL MHC-I tetramer$^+$ CD8α^+ T cells from mice vaccinated at the tail base was significantly higher than the footpad injection (Figure 5a). Therefore, subcutaneous vaccination at the tail base was adopted for the following animal experiments. To demonstrate that the external magnetic field enhances SIM-micelle enrichment in lymph nodes, we compared the vaccinated mice by SIM-micelles with or without application of an external magnetic field, which are denoted as SIM-micelle and SIM-micelles + mag (magnet) groups, respectively. After vaccination *in vivo*, it was found that the costimulatory markers CD40, MHC-1 H2-K^b SIINFEKL, and proinflammatory cytokines TNF-α and IFN-γ were significantly upregulated by SIM-micelles compared to other formulations, demonstrating the potency of SIM-micelles for the maturation of dendritic cells and promotion of antigen presentation in the inguinal lymph nodes (Figure 5b−e). We further assessed the expression of calreticulin (CRT) in lymphocytes induced by SIM-micelles *in vivo*, considering that Zn^{2+} can promote the expression of this protein.[37,56,57] Calreticulin (CRT) is involved not only with the folding of MHC class I molecules and their assembly factor tapasin but also the cell surface expression of MHC class I molecules, which are important for antigen presentation to cytotoxic T cells.[58−60] We found that the expression of calreticulin induced by SIM-micelles + mag was significantly higher than in other groups (Figure S10). Notably, the SIM-micelles + mag group had a significantly higher maturation and presentation level than the SIM-micelle group and others because the magnetic force facilitated SIM-micelles migrating to lymph nodes, leading to more enrichment in lymph nodes and the stimulation of lymphocytes (Figure 5b−e). Moreover, the generation of SIINFEKL-specific cytotoxic T lymphocytes was studied after mice were immunized with SIM-micelles. As shown in Figure 5f−g, compared with controls, SIM-micelles promoted the generation of more T cells specific for a variety of tumor antigens. The stronger T-cell responses *in vivo* induced by SIM-micelles may benefit from the dual adjuvants of $Zn_{1.15}Fe_{1.85}O_4$ and OA-R837 and efficient delivery and rapid traceless release of the antigen OVA peptide. Similarly, the T-cell responses in the SIM-micelles + mag group in the presence of the external magnetic field for 24 h were further improved, resulting from stronger magnetic-mediated codelivery of antigen and dual adjuvants to dLNs for the stronger enrichment in lymph nodes.

2.6. Anticancer Efficacy of SIM-Micelles. Next, the therapeutic efficacy of SIM-micelles was investigated. C57BL/6 mice were subcutaneously injected with 1×10^6 B16OVA cells on the back, and after 7 and 14 days, mice were immunized by SIM-micelles. The SIM-micelles + mag group

https://doi.org/10.1021/acs.chemmater.1c03681
Chem. Mater. 2021, 33, 9780−9794

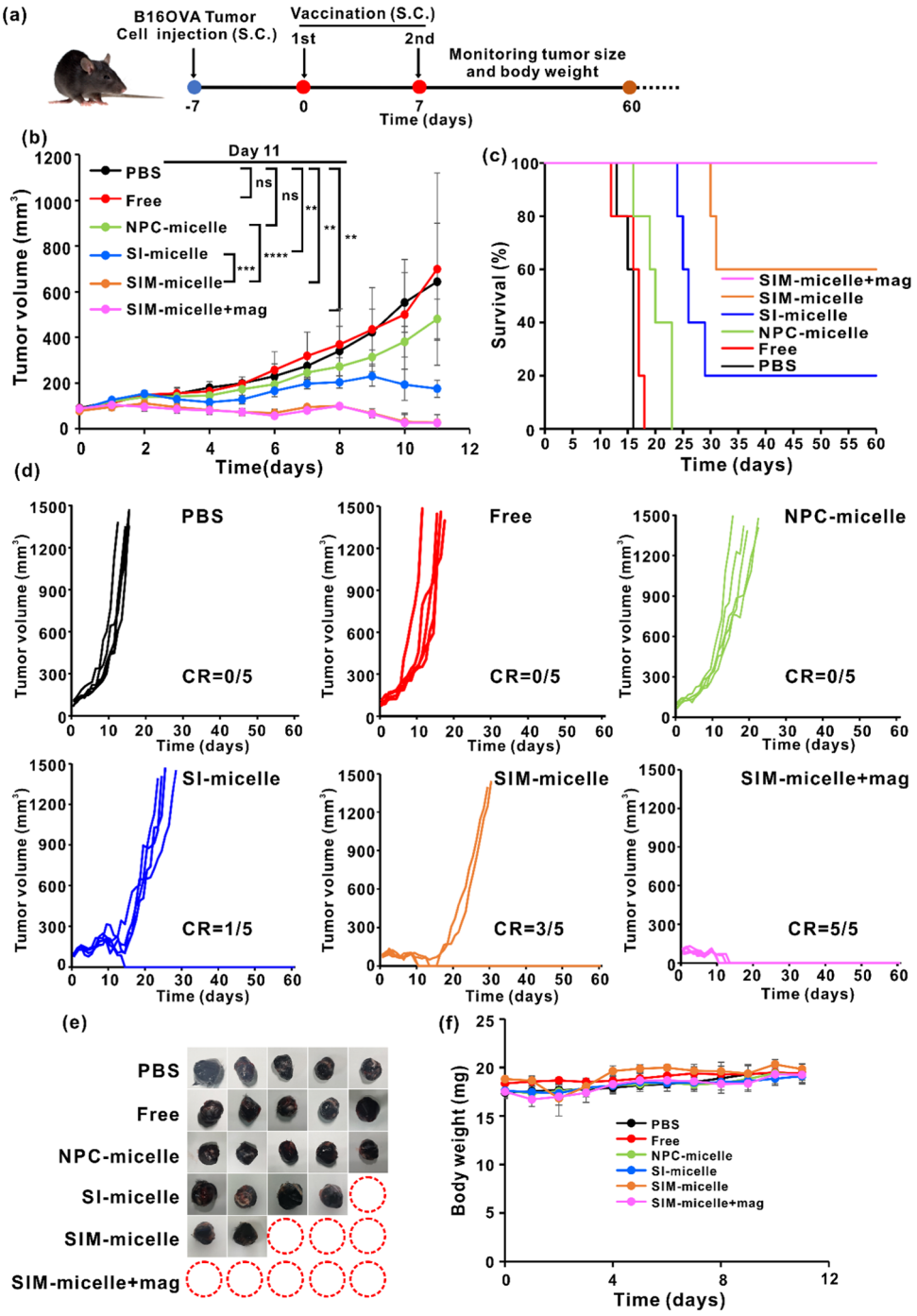

Figure 6. Therapeutic efficacy of SIM-micelles. B16-F10 cell-challenged mice were treated with PBS, free, NPC-micelles, SI-micelles, SIM-micelles, or SIM-micelles + mag. (a) Treatment scheme of tumor immunotherapy by SIM-micelles + mag. (b) Average tumor sizes before any of the mice died (n = 3; mean ± SD). (c) Survival rate over time (n = 5; mean ± SD). (d) Individual tumor growth kinetics over time (n = 5; mean ± SD). (e) Images of the dissected tumor tissues on day 30. Red circles mean that tumors were eradicated and unnoticeable and mice were left to be monitored until 60 days (n = 3; mean ± SD). (f) Body weight of mice treated with different formulations (n = 5; mean ± SD). One-way ANOVA analysis with two-tailed unpaired Student's t-test was used for significant difference analysis, $^{*}P < 0.05$, $^{**}P < 0.01$, $^{***}P < 0.001$, and $^{****}P < 0.0001$.

was treated with the magnetic field for 24 h after each immunization (Figure 6a). It was found that the vaccine-treated group had significantly better outcomes than the PBS group. Four out of five tumor-bearing mice in the SIM-micelle group were successfully cured on the 12th day after immune stimulation. One of them relapsed on the 16th day, but the tumor growth rate was significantly slower than that of the PBS, NPC-micelle, and SI-micelle groups. Importantly, all of the five mice in the SIM-micelles + mag group were cured on the 12th day, with a survival rate of 100% and no tumor recurrence occurred in all of the mice for at least 60 days (Figure 6b–e). During this entire period, the body weight of all mice did not show any significant change (Figure 6f). The potent tumor treatment efficacy of SIM-micelles + mag could

https://doi.org/10.1021/acs.chemmater.1c03681
Chem. Mater. 2021, 33, 9780−9794

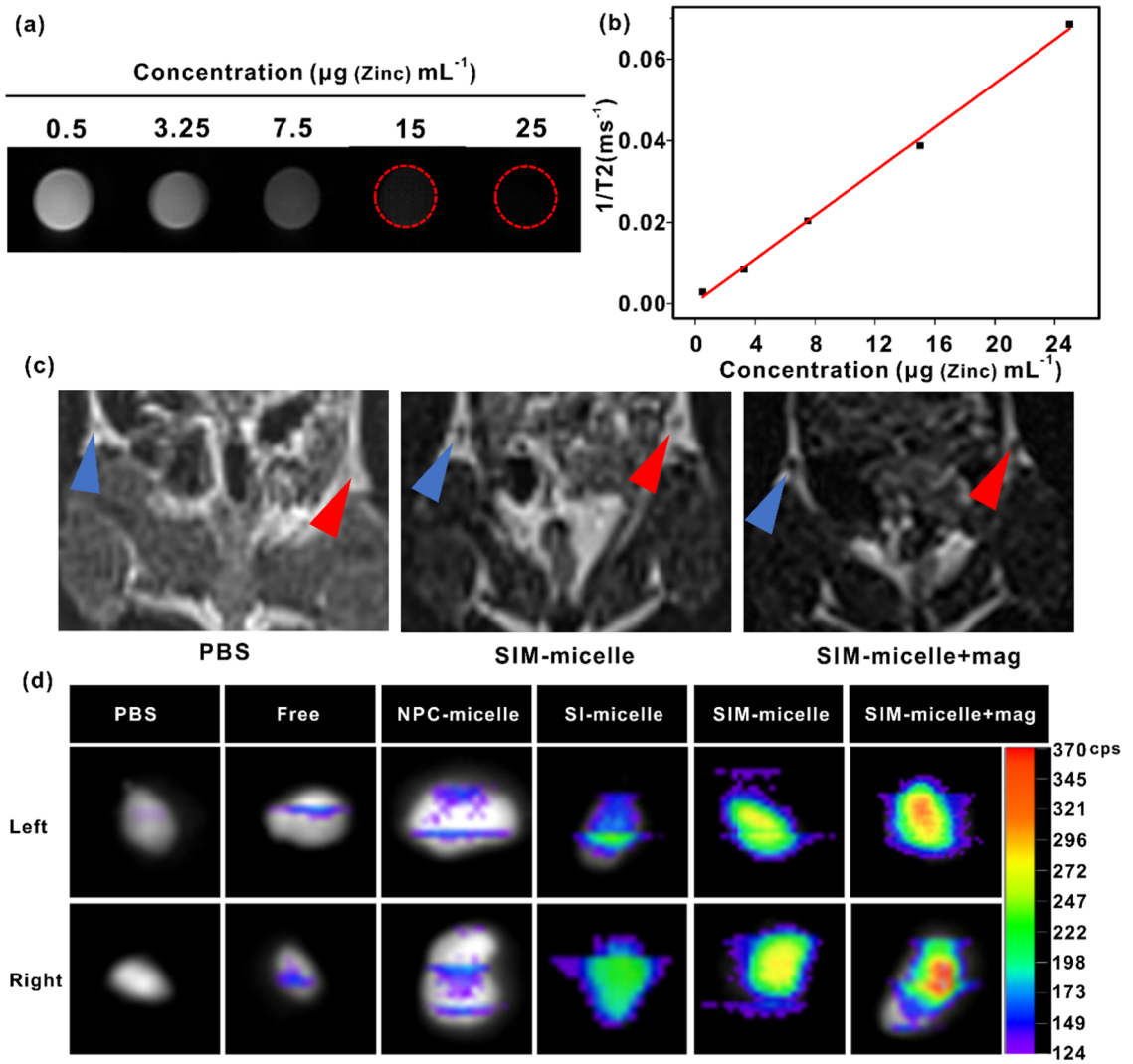

Figure 7. Lymph node imaging using magnetic SIM-micelles as contrast agents for tracking vaccine migration *in vivo*. (a) T_2-weighted phantom MRI of SIM-micelles with various concentrations. (b) Analysis of relaxation rate R_2 ($1/T_2$). (c) *In vivo* MRI images of draining inguinal lymph nodes 24 h after mice were subcutaneously injected PBS or SIM-micelles (treated with or without magnet). Blue and red arrows indicated right and left draining inguinal lymph nodes, respectively. (d) Near-infrared (NIR) fluorescence images of the draining inguinal ILNs acquired by the IVIS imaging system 24 h after mice were subcutaneously given FITC-labeled SIM-micelles. The concentration of $Zn_{1.15}Fe_{1.85}O_4$ was characterized by measuring the zinc ions by ICP-OES.

be explained by the enhanced delivery of SIM-micelles to dLNs by magnetic targeting. After the SIM-micelles reached lysosomes, the self-immolative linker quickly released antigen peptides and adjuvants, triggered by the lysosomal GSH, giving rise to strong immune responses to inhibit tumor growth and even eradicate tumors.

2.7. Lymph Node Imaging Using SIM-Micelles. In addition to the potent antitumor efficacy, the self-assembled magnetic nanovaccine can also act as a contrast agent for magnetic resonance imaging, enabling visualization and tracking of nanovaccine migration to dLNs. As shown in Figure 7a, SIM-micelles showed strong MRI contrast signals. Due to the shortening of T_2 relaxation, the signal intensity and relaxation time significantly reduced with increasing SIM-micelle concentrations, leading to darker images. The maximum saturation concentration of 25 μg mL^{-1} and a good correlation between the concentration and the MR signal are determined in Figure 7b. Taking advantage of the intrinsic MRI contrast of SIM-micelles, delivery of SIM-micelles in C57BL/6 mice *in vivo* could be monitored. The inguinal lymph nodes were imaged using a T_2-weighted multigradient echo MR sequence after 24 h injection of SIM-micelles. It was found that no MR signal was observed in mice treated with PBS, whereas the SIM-micelle group showed obvious MR signals, indicating that the magnetic SIM-micelles were successfully delivered to the inguinal lymph nodes (Figure 7c). In the SIM-micelles + mag group, further enhancement of the MR signal by the external magnetic field was observed, which again showed enhanced delivery of SIM-micelles to lymph nodes by a magnetic field (Figure 7c). In addition to MRI, the delivery of FITC-labeled SIM-micelles to lymph nodes can be imaged using fluorescence imaging. The SIM-micelles + mag group provided the strongest fluorescence intensity in the lymph nodes of vaccinated mice, but weaker fluorescence in the lymph nodes was seen in the SI-micelle, NPC-micelle, free, and PBS groups (Figure 7d). Taken together, this imaging theranostic nanoplatform can also be used to track the

https://doi.org/10.1021/acs.chemmater.1c03681
Chem. Mater. 2021, 33, 9780−9794

migration of the self-assembled magnetic nanovaccine to lymph nodes.

3. CONCLUSIONS

In summary, we developed a multifunctional self-assembled magnetic micelle system termed SIM-micelles for cancer vaccines. Both Inorganic $Zn_{1.15}Fe_{1.85}O_4$ and oleic acid-modified imiquimod R837 possessed immunostimulatory properties and were synergistically coencapsulated in Pluronic F127 polymeric micelles. F127 was chemically modified by an amine-containing and self-immolative linker, enabling the graft of antigen of OVA on micelles. Owing to the rapid and traceless release of the OVA and the dual adjuvants, magnetic SIM-micelles, assisted by an external magnetic field, effectively produced strong immune responses and eradicated tumors with a survival rate of 100% without recurrence for at least two months in a murine tumor model. In addition, the self-assembled magnetic nanovaccine micelles could be used as contrast agents to monitor the delivery of vaccines to the lymph node. This work demonstrates the potential of multifunctional SIM-micelles as a new class of biomaterials for cancer metalloimmunotherapy. The mouse tumor model used in this work is sensitive to modest amounts of OVA-specific cytotoxic lymphocytes; therefore, further investigation using other tumor models is needed. Future work also includes the adaption of SIM-micelle to present whole proteins or multiple peptides.

4. METHOD

4.1. Materials and Reagents. Pluronic F127 (Sigma). Antigen peptide $OVA_{257-264}$ (SIINFEKL) (GenScript, Nanjing, China). Imiquimod R837(Aladdin, Shanghai, China). Dithiodiglycolic acid (Jiuding Chemical, Shanghai, China). 4-Dimethylaminopyridine (Yuanye Bio-Technology, Shanghai, China). 1-(3-Dimethylaminopropyl)-3-ethylcarbodiimide hydrochloride (Meryer Chemical Technology, Shanghai, China). $FeCl_3{\cdot}6H_2O$ (Heowns, Tianjin, China). Sodium oleate (Heowns, Tianjin, China). Zinc oleate (Heowns, Tianjin, China). 1-Octadecene (Heowns, Tianjin, China). Tris(2-carboxyethyl) phosphine hydrochloride (Heowns, Tianjin, China). Glutathione (GSH) (Heowns, Tianjin, China). Fluorescein isothiocyanate (FITC) (Solarbio, Beijing, China). Antibodies against mouse CD11c-APC (catalogue no. 117309) (Biolegend, California). Anti-CD40-FITC (catalogue no. 102905) (Biolegend, California). Anti-CD86-PercpCy5.5 (catalogue no. 105027) (Biolegend, California). Anti-CD8a-APC (catalogue no. 100712) (Biolegend, California). Anti-CD3-FITC (catalogue no. 100203) (Biolegend, California). Antibodies against mouse H-$2K^b$ bound to SIINFEKL-PE-Cy7 (catalogue no. eBio25-D1.16) (Invitrogen, California). MHC I-strep for SIINFEKL (catalogue no. 6-7015-001) (IBA Lifescience, Germany). PE-Strep-Tactin (catalogue no. 6-5000-001) (IBA Lifescience, Germany). Recombinant mouse GM-CSF (catalogue no. 415-ML-020) (R&D systems, Minnesota). Anti-Calreticulin-Alexa Fluor 594 Conjugate (Cell Signaling Technology, Boston). Interleukin-6 (IL-6) mouse enzyme-linked immunosorbent assay (ELISA) kit (catalogue no. SEKM-0034) (Solarbio, Beijing, China). Interleukin-1β (IL-1β) mouse ELISA kit (catalogue no. SEKM-0034) (Solarbio, Beijing, China). Tumor necrosis factor-α (TNF-α) mouse ELISA kit (catalogue no. SEKM-0034) (Solarbio, Beijing, China). Interferon-γ (IFN-γ) mouse ELISA kit (catalogue no. SEKM-0031) (Solarbio, Beijing, China). 4′,6-Diamidino-2-phenylindole (DAPI) (Solarbio, Beijing, China). CCK-8 cell viability kit (Solarbio, Beijing, China). LysoTracker Red (catalogue no. C1046) (Beyotime Biotechnology, Shanghai, China).

4.2. Cell Lines. DC2.4 cells were purchased from the Beijing Beina Chuanglian Institute of Biotechnology. B16OVA cells were obtained from professor Shaokai Sun. The cells were cultured in 1640 medium with 100 U mL^{-1} of streptomycin, 100 U mL^{-1} of penicillin, and 10% FBS at 37 °C in a humidified incubator with 5% CO_2.

4.3. Animals. All studies performed on animals were approved; female C57BL/6 mice of age 6−8 weeks were purchased from Beijing Vital River Laboratory Animal Technology Co., Ltd. Mice were housed in groups of five mice per individually ventilated cage in a 12 h light−dark cycle (8:00−20:00 light; 20:00−8:00 dark), with constant room temperature (21 ± 1 °C) and relative humidity (40−70%). All the animal procedures were approved by the Animal Experiment Ethics Committee at the Tianjin University (permit number: TJUE-2021-025).

4.4. Preparation of $Zn_{1.15}Fe_{1.85}O_4$. A total of 5 mmol $FeCl_3{\cdot}6H_2O$, 15 mmol sodium oleate, 20 mL of absolute ethanol, 15 mL of deionized water, and 30 mL of hexane were added to the round-bottom flask successively and stirred at 70 °C under reflux for 4 h. After cooling to room temperature, the liquid was collected, then the oily substance in the upper layer was extracted three times with distilled water. The iron oleate was obtained as a red-brown waxy oily solid after drying in a vacuum. The synthesis of zinc oleate is similar to that of iron oleate, and white zinc oleate is obtained with $ZnCl_2$ and sodium oleate as precursors. Both zinc oleate and iron oleate were stored at room temperature for subsequent reactions.

A total of 1 mmol zinc oleate and 1.6 mmol iron oleate were dissolved in 15 mL of 1-octadecene, with the addition of 1.3×10^{-3} mol oleic acid. Then, the mixture was purged with Ar and heated to 120 °C to remove air for 30 min, then subjected to reflux and stirring at 320 °C for 2 h. After cooling to room temperature, isopropanol was added for precipitation, and then centrifugation was conducted at 6000 rpm for 10 min. $Zn_{1.15}Fe_{1.85}O_4$ was obtained after being washed three times with isopropanol. $Zn_{1.15}Fe_{1.85}O_4$ obtained by magnetic separation was dispersed in tetrahydrofuran and stored in a refrigerator at 4 °C for subsequent experiments. The morphology of $Zn_{1.15}Fe_{1.85}O_4$ was observed using a transmission electron microscope (JEM-F200, JEOL).

4.5. Preparation of Oleic Acid-Modified Imiquimod (R837). To increase the loading rate of R837, R837 is hydrophobically modified by oleic acid *via* the reaction of the amine group on R837 and oleoyl chloride. Specifically, 0.25 mmol R837 (1 equiv) and 0.3 mmol oleoyl chloride (1.2 equiv) were dissolved in 25 mL of anhydrous *N*,*N*-dimethylformamide and 58 μL of *N*,*N*-diisopropylethylamine (1.3 equiv). Under the protection of Ar, the mixture was stirred in a water bath at 70 °C for 12 h. A total of 100 mL of distilled water was added to remove the solvent *N*,*N*-dimethylformamide and unreacted oleyl chloride, and 125 mL of dichloromethane was added for extraction, the lower layer dichloromethane solution was collected, and the above operation was repeated twice. Thin-layer chromatographic separation was carried out with a developing solvent of dichloromethane and methanol (vol/vol = 10:1). Oleic acid-modified R837 (OA-R837) was obtained as the oily substance

https://doi.org/10.1021/acs.chemmater.1c03681
Chem. Mater. 2021, 33, 9780−9794

and was characterized by NMR (JEOL JNM ECZ600R). OA-R837 was dissolved in tetrahydrofuran for further use.

4.6. Preparation of Self-Immolative Magnetic Micellar Vaccines. To synthesize F127-SH, 0.1 mmol pristine F127, 0.8 mmol dithiodiglycolic acid, 0.8 mmol 1-(3-dimethylaminopropyl)-3-ethylcarbodiimide hydrochloride, and 0.8 mmol 4-dimethylaminopyridine were dissolved in 20 mL of dichloromethane and stirred for 12 h. The resulting solution was precipitated in cold ether on ice, and the precipitate was collected by centrifugation at 3000 rcf for 30 min. The precipitate was added in a 6000−8000 Da dialysis bag for dialysis against distilled water, and the buffer was changed 3 times every 6−8 h. A total of 1.59 mmol tris(2-carboxyethyl) phosphine hydrochloride and 220 μL of triethylamine were added to the dialysate for reaction overnight without oxygen. After dialysis, the resulting liquid was freeze-dried to obtain F127-SH as a pale-yellow solid, which was stored in a refrigerator at −20 °C for further use. A self-immolative linker was synthesized and characterized according to our previously published results.[61]

To synthesize self-immolative linker-modified F127, 0.02 mmol F127-SH and 0.05 mmol self-immolative linker was dissolved in 20 mL of dichloromethane and stirred overnight. After removing dichloromethane, 20 mL of distilled water was added for extraction. The water solution was collected and freeze-dried to obtain self-immolative linker-modified F127 (termed SI-F127). To demonstrate the advantages of the self-immolative linker that can release pristine OVA rapidly, we synthesized nonimmolative NPC-F127 as a control as well. Briefly, 1.005 g of *p*-nitrophenyl chloroformate (NPC) and 10 g of dehydrated Pluronic F127 were dissolved in 35 mL of benzene with stirring for 24 h at 25 °C under Ar, then NPC-F127 was collected after rotary evaporation and precipitation in cold diethyl ether.[62]

To encapsulate $Zn_{1.15}Fe_{1.85}O_4$ and OA-R837 in SI-F127 or NPC-F127 micelles, generating SIM-micelles (self-immolative magnetic micelles containing $Zn_{1.15}Fe_{1.85}O_4$ and OA-R837 and OVA) and NPC-micelles (nonimmolative micelles containing $Zn_{1.15}Fe_{1.85}O_4$ and OA-R837 and OVA as control), 60 μL of $Zn_{1.15}Fe_{1.85}O_4$ (8 mg mL^{-1}) and 30 μL of OA-R837 (3 mg mL^{-1}) tetrahydrofuran solution were quickly injected into 1 mL of 5 wt % SI-F127 or NPC-F127 aqueous solution. The mixture was sonicated for 3 min and then the tetrahydrofuran was removed by rotary evaporation. Afterward, the unincorporated or free micelles were removed by ultrafiltration at low temperatures, and the $Zn_{1.15}Fe_{1.85}O_4$ and OA-R837 were quantitatively analyzed by inductively coupled plasma optical emission spectrometry (ICP-OES) (iCAP7000 series) and a microplate reader (excitation = 250 nm, emission = 354 nm) (Infinite 200Pro), respectively. For the conjugation of OVA on the surface of micelles, 8 μL of $OVA_{257-264}$ (5 mg mL^{-1}) was mixed with the concentrated OA-R837 and $Zn_{1.15}Fe_{1.85}O_4$-encapsulated SI-F127 micelle (20 μg of OA-R837 and 20 μg of $Zn_{1.15}Fe_{1.85}O_4$) aqueous solution. Then, 10 μL of NaOH (1 mol L^{-1}) was added to adjust the pH to around 9−10 and then the mixture was stirred for 30 min in the dark, and unreacted OVA was removed by ultrafiltration. FITC-labeled OVA is measured using a microplate reader to detect the fluorescence intensity of FITC-labeled OVA (excitation = 450 nm, emission = 520 nm). The micellar vaccines of SI-F127-$Zn_{1.15}Fe_{1.85}O_4$-OA-R837-OVA and NPC-F127-$Zn_{1.15}Fe_{1.85}O_4$-OA-R837-OVA were obtained and denoted as SIM-micelles and NPC-micelles, respectively. The preparation of the control group denoted as SI-micelles was the same as SIM-micelles except adding OA-R837 only but no $Zn_{1.15}Fe_{1.85}O_4$ in the core of micelles. The mixture of free OA-R837 and OVA was denoted free, whereas the mixture of free R837 (without OA modification) and OVA was denoted as free (−). The morphology of micelles was observed using a transmission electron microscope (JEM-F200, JEOL) and a Zeiss thermal scanning electron microscope (Sigma, 300). The magnetic properties of micelles are obtained using a vibrating sample magnetometer (BKT-4500).

4.7. *In Vitro* Release of OVA and Zinc Ions. To study the OVA release in the presence of GSH, 1 mL of NPC-micelles or SIM-micelles, OVA = 33 μg mL^{-1} was placed in a dialysis bag (molecular weight cut off: 5000 Da) against 35 mL of 0.01 M phosphate buffer solution (with or without 10 mM GSH). At predetermined time points (10, 20, 30, 40, 60, 120, 240 min), 1 mL of the buffer outside the dialysis bag was taken out for the quantification of OVA by high-performance liquid chromatography (HPLC) (1260 Infinity II).

To study the zinc ion release, SIM-micelles were diluted to 7.5 μg mL^{-1} (zinc concentration) by 1 mL of buffer solution (pH = 5 or 7) containing with or without 10 mM GSH, followed by incubation at 37 °C for different times. The solutions were then centrifuged at high speed (14 000 rcf, 4 °C, 40 min), and the supernatant was collected for nitrification using aqua regia. The concentration of zinc ions released from the micelles was quantified by ICP-OES.

4.8. Bone Marrow-Derived Dendritic Cell (BMDC) Extraction. To collect BMDCs, female C57BL/6 mice at the age of 6−8 weeks were sacrificed and the femur was then taken out and washed with 75% alcohol and PBS, and both ends were cut off. Bone marrow was then flushed out of the bone with a 1 mL sterile syringe using warm BMDC basal media consisting of 500 mL of Roswell Park Memorial Institute (RPMI) 1640 with 2 mM L-glutamine and 25 mM 4-(2-hydroxyethyl)-1-piperazineethanesulfonic acid (HEPES) supplemented with 50 mL of fetal bovine serum (Yesen) and 5 mL of penicillin−streptomycin. After the cells were collected by centrifugation (1000 rpm, 5 min), 1 mL of red blood cell lysate (Solarbio) was added to lyse the cells on ice for 3 min. BMDC cells were collected again by centrifugation (1000 rpm, 5 min). Then, 1×10^6 cells mL^{-1} and 1640 medium containing a granulocyte/macrophage-colony stimulating factor (GM-CSF, R&D) were added to cell culture dishes and incubated at 37 °C with 5% CO_2. On the third day of cell culture, 10 mL of BMDC growth medium was added to each dish.

4.9. *In Vitro* Uptake, Cell Viability, and Antigen Localization. For the study of *in vitro* cellular uptake, 1×10^5 DC2.4 mL^{-1} was incubated with the following formulations including free formulation (containing 2 μg mL^{-1} OVA + 4.5 μg mL^{-1} OA-R837 + 7.5 μg (zinc) mL^{-1} $Zn_{1.15}Fe_{1.85}O_4$); NPC-micelles (containing 2 μg mL^{-1} OVA + 4.5 μg mL^{-1} OA-R837 + 7.5 μg (zinc) mL^{-1} $Zn_{1.15}Fe_{1.85}O_4$); SI-micelles (containing 2 μg mL^{-1} OVA + 4.5 μg mL^{-1} OA-R837); and SIM-micelles (containing 2 μg mL^{-1} OVA + 4.5 μg mL^{-1} OA-R837 + 7.5 μg (zinc) mL^{-1} $Zn_{1.15}Fe_{1.85}O_4$) in 24-well plates at 37 °C with 5% CO_2 for different times (0, 0.5, 1.5, 2, 3, 5, 7, 9, 11, 25 h). After the cells were lysed with 1% Triton X-100, the fluorescence intensity of FITC-labeled OVA was measured with a microplate reader (excitation = 450 nm, emission = 520 nm).

To investigate the antigen localization by a confocal microscope, DC2.4 cells were first seeded into a confocal culture dish at a concentration of 1×10^6 cells mL^{-1}. The

https://doi.org/10.1021/acs.chemmater.1c03681
Chem. Mater. 2021, 33, 9780−9794

DC2.4 cells were then incubated with the following formulations, including free formulation (containing 2 μg mL^{-1} OVA + 4.5 μg mL^{-1} OA-R837 + 7.5 μg (zinc) mL^{-1} $Zn_{1.15}Fe_{1.85}O_4$); NPC-micelles (containing 2 μg mL^{-1} OVA + 4.5 μg mL^{-1} OA-R837 + 7.5 μg (zinc) mL^{-1} $Zn_{1.15}Fe_{1.85}O_4$); SI-micelles (containing 2 μg mL^{-1} OVA + 4.5 μg mL^{-1} OA-R837); and SIM-micelles (containing 2 μg mL^{-1} OVA + 4.5 μg mL^{-1} OA-R837 + 7.5 μg (zinc) mL^{-1} $Zn_{1.15}Fe_{1.85}O_4$), for 5 h. The cells were washed three times with PBS. DAPI (Solarbio) and LysoTracker Red (Beyotime Biotechnology) were used to stain the nucleus and lysosomes for 40 min. Intracellular fluorescence was observed under a confocal microscope.

Cell viability was measured using a CCK-8 kit. Twenty microliters of different concentrations of SIM-micelles or free formulations (containing 2 μg mL^{-1} OVA, 4.5 μg mL^{-1} OA-R837, and varying concentrations of $Zn_{1.15}Fe_{1.85}O_4$) with zinc ion concentrations of 0, 0.5, 2.5, 5, 7.5, 10.5, 15, 30, 45, and 60 μg mL^{-1} was incubated with 8 × 10^4 DC2.4 cells well^{-1} in a 96-well plate at 37 °C for 24 h. Then, 10 μL of CCK-8 solution was added to 96 wells and placed in an incubator at 37 °C for 4 h. The absorbance was measured at 450 nm using a Varioskan Flash (Thermo Scientific).

4.10. Dendritic Cell Activation *In Vitro*. In this experiment, the following formulations were used: free formulation (containing 2 μg mL^{-1} OVA + 4.5 μg mL^{-1} OA-R837 + 7.5 μg (zinc) mL^{-1} $Zn_{1.15}Fe_{1.85}O_4$); free (−) formulation is similar to free formulation but just replacing OA-R837 with unmodified R837; NPC-micelles (containing 2 μg mL^{-1} OVA + 4.5 μg mL^{-1} OA-R837 + 7.5 μg (zinc) mL^{-1} $Zn_{1.15}Fe_{1.85}O_4$); SI-micelles (containing 2 μg mL^{-1} OVA + 4.5 μg mL^{-1} OA-R837); and SIM-micelles (containing 2 μg mL^{-1} OVA + 4.5 μg mL^{-1} OA-R837 + 7.5 μg (zinc) mL^{-1} $Zn_{1.15}Fe_{1.85}O_4$).

Dendritic cell activation following immunization with various vaccine formulations was determined by measuring dendritic cell maturation markers and lymph node cytokine secretion. To analyze markers of dendritic cell maturation, 2 mL of 1 × 10^6 BMDCs mL^{-1} was seeded in six-well plates. After 200 μL of various vaccine formulations was added, the cells were placed in an incubator at 37 °C for 24 h. The BMDCs were collected by centrifugation (1900 rpm, 8 min) and incubated with an anti-APC-CD11c antibody, anti-FITC-CD40 antibody, anti-PE-Cy5.5-CD86 antibody, and anti-PE-Cy7-MHC I antibody. The cells were then washed twice with PBS, resuspended in PBS, and analyzed by flow cytometry. Data were collected using a Becton Dickinson FACS Aria III flow cytometer and analyzed using FlowJo software. To analyze cytokine, 2 mL of 1 × 10^6 DC2.4 mL^{-1} was incubated with 200 μL of PBS or different vaccine formulations. The supernatant was collected by centrifugation (1000 rpm, 5 min). The concentrations of proinflammatory cytokines were measured with IL-6, IL-1β, TNF-α, and IFN-γ ELISA kits (Solarbio) according to protocols provided by manufacturers.

4.11. *In Vitro* Migration Assay. BMDCs were cultured as described above and plated at 50% confluency in a 25 cm^2 culture dish. Different concentrations of SIM-micelles (zinc ion = 0, 0.5, 3.25, 7.5 μg mL^{-1}) were added to the culture dish and incubated for 5 h, and then the cell magnetic migration study was carried out in a six-well transwell culture chamber (8 μm). Fresh 1640 medium was placed (without FBS) in the lower chamber, and the BMDCs (1 × 10^7 cells per 100 μL) preincubated with SIM-micelles were placed in the upper chamber. The magnet treatment was performed with a magnet (120 × 80 × 10 mm^3) placed under the six-well culture chamber. After 2 h of incubation, the cells that migrated to the lower chamber were counted by a hemocytometer.

4.12. Imaging of Draining Inguinal Lymph Nodes. Female C57BL/6 mice were subcutaneously injected at tail base PBS and various FITC-labeled $OVA_{257-264}$ formulations, including free, NPC-micelles, SI-micelles, and SIM-micelles (OVA = 20 μg, OA-R837 = 20 μg, zinc ion = 20 μg per mouse), at the tail base. In addition, another group named SIM-micelles + mag is the same as the SIM-micelle group, except that a ring magnet (14 × 4 mm^2) was put around the waist after vaccination. After 24 h, draining inguinal lymph nodes on both sides were harvested and the fluorescence signal of FITC in different groups was recorded by the IVIS optical imaging system (NIGHT OWL IILB983, Berthold Technologies).

In Figure 7a,b, MR images of SIM samples were acquired with a 1.2 T HT/MRSI60-60KY. The 1.2 T MRI rat imaging research system was used to observe the MRI effects of the samples with different concentrations (zinc ion = 0.5, 3.25, 7.5, 15, 25 μg mL^{-1}). The acquisition parameters used were: repetition time (TR)/echo time (TE) = 5000/52.8 ms, field of view (FOV) = 50 × 80 mm^2, matrix = 512 × 256, slice thickness = 0.4 mm, 30 °C, and NEX = 256. In Figure 7c, MRI images of draining inguinal LNs were acquired using 3.0 T MAGNETOM Spectra. The MR images of lymph nodes *ex vivo* were acquired using the following sequence parameters: MSME 2200/101 ms (TR/TE), 11 slices with a thickness of 1.0 mm, a FOV of 2.3 × 2.3 cm^2, a matrix of 230 × 230, and NEX = 1. The same image protocols were adopted for *in vivo* imaging. Female C57BL/6 mice were injected subcutaneously with 200 μL of PBS or SIM-micelle sample (OVA = 20 μg, OA-R837 = 20 μg, zinc ion = 20 μg per mouse). The SIM+ group was treated similarly as the SIM group but with a ring magnet (14 × 4 mm^2) put around the mouse waist for 24 h.

4.13. *In Vivo* Immunization and Cancer Immunotherapy Studies. Female C57BL/6 mice of age 6−8 weeks were subcutaneously immunized with different formulations, including PBS, free (OVA + OA-R837 + $Zn_{1.15}Fe_{1.85}O_4$), NPC-micelles (OVA + OA-R837 + $Zn_{1.15}Fe_{1.85}O_4$), SI-micelles (OVA + OA-R837 but without $Zn_{1.15}Fe_{1.85}O_4$), and SIM-micelles (OVA + OA-R837 + $Zn_{1.15}Fe_{1.85}O_4$). All of the formulations contained the same concentrations of $OVA_{257-264}$ (20 μg per mouse), OA-R837 (20 μg per mouse), and $Zn_{1.15}Fe_{1.85}O_4$ (20 μg per mouse) unless otherwise noted in 200 μL volume. The SIM-micelle + mag group is the same as the SIM group, except adding a ring magnet (14 × 4 mm^2) around the mouse waist for 24 h. After 7 days, peripheral blood and inguinal lymph nodes were collected for the measurement of cytokines, specific CD8$^+$ T cells, dendritic cell maturation markers, and calreticulin expression. To quantify cytokines, the peripheral blood was centrifuged (4 °C, 1000 rcf, 10 min) to collect serum. TNF-α and IFN-γ ELISA kits were used to detect serum cytokine levels according to the manufacturer's instructions. Peripheral blood was lysed with red blood cell lysate (Solarbio) at 4 °C for 5 min, and then the cells were collected and stained with a PE-conjugated tetramer, FITC-conjugated CD3, and APC-conjugated CD8. Specific CD8$^+$ T cells were labeled. Data were collected using a Becton Dickinson FACS Aria III flow cytometer and analyzed using FlowJo software. To examine the dendritic cell maturation *in vivo* and the expression of calreticulin in lymphocytes, the

https://doi.org/10.1021/acs.chemmater.1c03681
Chem. Mater. 2021, 33, 9780−9794

inguinal lymph nodes were collected and ground into a single cell suspension, and the cells were collected by centrifugation (1400 rpm, 5 min). A part of the cells was stained using an anti-APC-CD11c antibody, anti-FITC-CD40 antibody, and anti-PE-Cy7-MHC I antibody. Another part of the cell was stained with Alexa Fluor 594-labeled CRT antibody. After incubation at 4 °C for 30 min, the cells were washed with PBS three times. Data were collected using a Becton Dickinson FACS Aria III flow cytometer and analyzed using FlowJo software.

4.14. Therapeutic Efficacy. Female C57BL/6 mice of age 6−8 weeks were subcutaneously injected 1×10^6 B16OVA cells per mouse on the right flank. Body weight and tumor size were measured every day. Tumor volume was calculated as width^2 × length × 0.5. When the tumor volume reached approximately 100 mm^3, the mice were randomly divided into six groups (five mice per group). The mice were injected subcutaneously with PBS, free, NPC-micelles, SI-micelles, or SIM-micelles. After 7 days, various formulations were injected again. In addition, the SIM-micelles + mag group was treated similarly as the SIM group but by putting a ring magnet around the waist of mice for 24 h. Mice were sacrificed when the tumor size reached 1500 mm^3 or when animals became moribund with severe weight loss or ulceration.

■ ASSOCIATED CONTENT

Supporting Information

The Supporting Information is available free of charge at https://pubs.acs.org/doi/10.1021/acs.chemmater.1c03681.

Description of the synthetic route of materials and ^{1}H NMR spectrum; fluorescence spectra of R837 and OA-R837; schematic illustration of SI-micelles and NPC-micelles; detailed components of different formulations; $Zn_{1.15}Fe_{1.85}O_4$ loading amount; HPLC analysis for OVA; and release of $OVA_{257-264}$ and Zn^{2+} from SIM-micelles with 1 U esterase or 10 mM GSH and CRT^+ cell percentage of lymphocytes cells (PDF)

■ AUTHOR INFORMATION

Corresponding Author

Yumiao Zhang − *Key Laboratory of System Bioengineering (Ministry of Education), School of Chemical Engineering and Technology, Tianjin University, Tianjin 300350, China; Institute of Shaoxing, Tianjin University, Zhejiang 312300, China;* orcid.org/0000-0002-6166-0470; Email: ymzhang88@tju.edu.cn

Authors

Jiexin Li − *Key Laboratory of System Bioengineering (Ministry of Education), School of Chemical Engineering and Technology, Tianjin University, Tianjin 300350, China*

He Ren − *Key Laboratory of System Bioengineering (Ministry of Education), School of Chemical Engineering and Technology, Tianjin University, Tianjin 300350, China*

Yaping Sun − *Imaging Center, Tianjin Beichen District Hospital of Traditional Chinese Medicine, Tianjin 300350, China*

Gengqi Liu − *Key Laboratory of System Bioengineering (Ministry of Education), School of Chemical Engineering and Technology, Tianjin University, Tianjin 300350, China*

Xingyue Yang − *Key Laboratory of System Bioengineering (Ministry of Education), School of Chemical Engineering and Technology, Tianjin University, Tianjin 300350, China*

Qian Qiu − *Key Laboratory of System Bioengineering (Ministry of Education), School of Chemical Engineering and Technology, Tianjin University, Tianjin 300350, China*

Yuanmeng Ding − *Key Laboratory of System Bioengineering (Ministry of Education), School of Chemical Engineering and Technology, Tianjin University, Tianjin 300350, China*

Jonathan F. Lovell − *Department of Biomedical Engineering, The State University of New York at Buffalo, Buffalo, New York 14260, United States;* orcid.org/0000-0002-9052-884X

Complete contact information is available at: https://pubs.acs.org/10.1021/acs.chemmater.1c03681

Author Contributions

J.L. and Y.Z. conceived the project. J.L. carried out most experiments. H.R. and G.L. assisted with material synthesis and animal experiments. Y.S. assisted with MRI experiments of lymph nodes. X.Y., Q.Q., and Y.D. assisted with material synthesis and characterization. J.F.L. assisted with manuscript editing. J.L. and Y.Z. performed data analysis and wrote the manuscript.

Funding

This work was supported by the National Key Research and Development Program (2021YFC2102300), the National Natural Science Foundation of China (32071384), and the Start-up Grant at Tianjin University and One-Thousand Young Talent Program of China.

Notes

The authors declare no competing financial interest.

■ ACKNOWLEDGMENTS

The authors thank Professor Shaokai Sun for kindly providing B16OVA cells, Shaolan Zou for the assistance with flow cytometry testing, and Lixia Long for the assistance with confocal microscopic imaging.

■ REFERENCES

(1) Mellman, I.; Coukos, G.; Dranoff, G. Cancer immunotherapy comes of age. *Nature* **2011**, *480*, 480−489.

(2) Ganesh, K.; Stadler, Z. K.; Cercek, A.; Mendelsohn, R. B.; Shia, J.; Segal, N. H.; Diaz, L. A., Jr. Immunotherapy in colorectal cancer: rationale, challenges and potential. *Nat. Rev. Gastroenterol. Hepatol.* **2019**, *16*, 361−375.

(3) Li, H.; Gu, Z. Nanodevices for cancer vaccination. *Nat. Mater.* **2021**, *20*, 286−287.

(4) Zhang, C.; Pu, K. Molecular and nanoengineering approaches towards activatable cancer immunotherapy. *Chem. Soc. Rev.* **2020**, *49*, 4234−4253.

(5) Moon, J. J.; Suh, H.; Bershteyn, A.; Stephan, M. T.; Liu, H.; Huang, B.; Sohail, M.; Luo, S.; Um, S. H.; Khant, H.; Goodwin, J. T.; Ramos, J.; Chiu, W.; Irvine, D. J. Interbilayer-crosslinked multilamellar vesicles as synthetic vaccines for potent humoral and cellular immune responses. *Nat. Mater.* **2011**, *10*, 243−251.

(6) Han, X.; Shen, S.; Fan, Q.; Chen, G.; Archibong, E.; et al. Red blood cell−derived nanoerythrosome for antigen delivery with enhanced cancer immunotherapy. *Sci. Adv.* **2019**, *5*, No. eaaw6870.

(7) He, S.; Li, J.; Cheng, P.; Zeng, Z.; Zhang, C.; Duan, H.; Pu, K. Charge-Reversal Polymer Nano-modulators for Photodynamic Immunotherapy of Cancer. *Angew. Chem., Int. Ed.* **2021**, *60*, 19355−19363.

(8) Heuts, J.; Varypataki, E. M.; van der Maaden, K.; Romeijn, S.; Drijfhout, J. W.; van Scheltinga, A. T.; Ossendorp, F.; Jiskoot, W. Cationic Liposomes: A Flexible Vaccine Delivery System for Physicochemically Diverse Antigenic Peptides. *Pharm. Res.* **2018**, *35*, No. 207.
(9) Gong, N.; Zhang, Y.; Teng, X.; Wang, Y.; Huo, S.; Qing, G.; Ni, Q.; Li, X.; Wang, J.; Ye, X.; et al. Proton-driven transformable nanovaccine for cancer immunotherapy. *Nat. Nanotechnol.* **2020**, *15*, 1053−1064.
(10) Xu, J.; Lv, J.; Zhuang, Q.; Yang, Z.; Cao, Z.; Xu, L.; Pei, P.; Wang, C.; Wu, H.; Dong, Z.; et al. A general strategy towards personalized nanovaccines based on fluoropolymers for post-surgical cancer immunotherapy. *Nat. Nanotechnol.* **2020**, *15*, 1043−1052.
(11) Nam, J.; Son, S.; Park, K. S.; Moon, J. J. Modularly Programmable Nanoparticle Vaccine Based on Polyethyleneimine for Personalized Cancer Immunotherapy. *Adv. Sci.* **2021**, *8*, No. 2002577.
(12) Farzad, N.; Barati, N.; Momtazi-Borojeni, A. A.; Yazdani, M.; Arab, A.; Razazan, A.; Shariat, S.; Mansourian, M.; Abbasi, A.; Saberi, Z.; Badiee, A.; Jalali, S. A.; Jaafari, M. R. P435 HER2/neu-derived peptide conjugated to liposomes containing DOPE as an effective prophylactic vaccine formulation for breast cancer. *Artif. Cells, Nanomed., Biotechnol.* **2019**, *47*, 664−672.
(13) Jacoberger-Foissac, C.; Saliba, H.; Seguin, C.; Brion, A.; Kakhi, Z.; Frisch, B.; Fournel, S.; Heurtault, B. Optimization of peptide-based cancer vaccine compositions, by sequential screening, using versatile liposomal platform. *Int. J. Pharm.* **2019**, *562*, 342−350.
(14) Nobs, L.; Buchegger, F.; Gurny, R.; Allemann, E. Current methods for attaching targeting ligands to liposomes and nanoparticles. *J. Pharm. Sci.* **2004**, *93*, 1980−1992.
(15) Jackson, D. C.; Drummer, H. E.; Urge, L.; Otvos, L., Jr.; Brown, L. E. Glycosylation of a synthetic peptide representing a T-cell determinant of influenza virus hemagglutinin results in loss of recognition by CD4+ T-cell clones. *Virology* **1994**, *199*, 422−430.
(16) Ghaffar, K. A.; Marasini, N.; Giddam, A. K.; Batzloff, M. R.; Good, M. F.; Skwarczynski, M.; Toth, I. Liposome-based intranasal delivery of lipopeptide vaccine candidates against group A streptococcus. *Acta Biomater.* **2016**, *41*, 161−168.
(17) Khongkow, M.; Liu, T.-Y.; Bartlett, S.; Hussein, W. M.; Nevagi, R.; Jia, Z.; Monteiro, M. J.; Wells, J.; Ruktanonchai, U. R.; Skwarczynski, M.; Toth, I. Liposomal formulation of polyacrylate-peptide conjugate as a new vaccine candidate against cervical cancer. *Precis. Nanomed.* **2018**, *1*, 183−193.
(18) He, X.; Zhou, S.; Huang, W. C.; Seffouh, A.; Mabrouk, M. T.; Morgan, M. T.; Ortega, J.; Abrams, S. I.; Lovell, J. F. A Potent Cancer Vaccine Adjuvant System for Particleization of Short, Synthetic CD8(+) T Cell Epitopes. *ACS Nano* **2021**, *15*, 4357−4371.
(19) Shao, S.; Geng, J.; Ah Yi, H.; Gogia, S.; Neelamegham, S.; Jacobs, A.; Lovell, J. F. Functionalization of cobalt porphyrin-phospholipid bilayers with his-tagged ligands and antigens. *Nat. Chem.* **2015**, *7*, 438−446.
(20) He, X.; Zhou, S.; Quinn, B.; Jahagirdar, D.; Ortega, J.; Abrams, S. I.; Lovell, J. F. HPV-Associated Tumor Eradication by Vaccination with Synthetic Short Peptides and Particle-Forming Liposomes. *Small* **2021**, *17*, No. 2007165.
(21) Wilson, D. S.; Hirosue, S.; Raczy, M. M.; Bonilla-Ramirez, L.; Jeanbart, L.; Wang, R.; Kwissa, M.; Franetich, J. F.; Broggi, M. A. S.; Diaceri, G.; Quaglia-Thermes, X.; Mazier, D.; Swartz, M. A.; Hubbell, J. A. Antigens reversibly conjugated to a polymeric glyco-adjuvant induce protective humoral and cellular immunity. *Nat. Mater.* **2019**, *18*, 175−185.
(22) Wilson, D. S.; Damo, M.; Hirosue, S.; Raczy, M. M.; Brunggel, K.; Diaceri, G.; Quaglia-Thermes, X.; Hubbell, J. A. Synthetically glycosylated antigens induce antigen-specific tolerance and prevent the onset of diabetes. *Nat. Biomed. Eng.* **2019**, *3*, 817−829.
(23) Yang, R.; Xu, J.; Xu, L.; Sun, X.; Chen, Q.; Zhao, Y.; Peng, R.; Liu, Z. Cancer Cell Membrane-Coated Adjuvant Nanoparticles with Mannose Modification for Effective Anticancer Vaccination. *ACS Nano* **2018**, *12*, 5121−5129.
(24) Li, S.; Feng, X.; Wang, J.; Xu, W.; Islam, M. A.; Sun, T.; Xie, Z.; Wang, C.; Ding, J.; Chen, X. Multiantigenic Nanoformulations Activate Anticancer Immunity Depending on Size. *Adv. Funct. Mater.* **2019**, *29*, No. 1903391.
(25) Michaelis, K. A.; Norgard, M. A.; Zhu, X.; Levasseur, P. R.; Sivagnanam, S.; Liudahl, S. M.; Burfeind, K. G.; Olson, B.; Pelz, K. R.; Angeles Ramos, D. M.; Maurer, H. C.; Olive, K. P.; Coussens, L. M.; Morgan, T. K.; Marks, D. L. The TLR7/8 agonist R848 remodels tumor and host responses to promote survival in pancreatic cancer. *Nat. Commun.* **2019**, *10*, No. 4682.
(26) Bahmani, B.; Gong, H.; Luk, B. T.; Haushalter, K. J.; DeTeresa, E.; Previti, M.; Zhou, J.; Gao, W.; Bui, J. D.; Zhang, L.; Fang, R. H.; Zhang, J. Intratumoral immunotherapy using platelet-cloaked nanoparticles enhances antitumor immunity in solid tumors. *Nat. Commun.* **2021**, *12*, No. 1999.
(27) Jiang, Y.; Huang, J.; Xu, C.; Pu, K. Activatable polymer nanoagonist for second near-infrared photothermal immunotherapy of cancer. *Nat. Commun.* **2021**, *12*, No. 742.
(28) Kuai, R.; Ochyl, L. J.; Bahjat, K. S.; Schwendeman, A.; Moon, J. J. Designer vaccine nanodiscs for personalized cancer immunotherapy. *Nat. Mater.* **2017**, *16*, 489−496.
(29) Kroll, A. V.; Fang, R. H.; Jiang, Y.; Zhou, J.; Wei, X.; Yu, C. L.; Gao, J.; Luk, B. T.; Dehaini, D.; Gao, W.; et al. Nanoparticulate Delivery of Cancer Cell Membrane Elicits Multiantigenic Antitumor Immunity. *Adv. Mater.* **2017**, *29*, No. 1703969.
(30) Li, H. Y.; Li, Y. H.; Jiao, J.; Hu, H. M. Alpha-alumina nanoparticles induce efficient autophagy-dependent cross-presentation and potent antitumour response. *Nat. Nanotechnol.* **2011**, *6*, 645−650.
(31) Sun, B.; Ji, Z.; Liao, Y.-P.; Wang, M.; Wang, X.; Dong, J.; Chang, C. H.; Li, R.; Zhang, H.; Nel, A. E.; Xia, T. Engineering an Effective Immune Adjuvant by Designed Control of Shape and Crystallinity of Aluminum Oxyhydroxide Nanoparticles. *ACS Nano* **2013**, *7*, 10834−10849.
(32) Chen, Q.; Sun, L.; Chen, Z. J. Regulation and function of the cGAS-STING pathway of cytosolic DNA sensing. *Nat. Immunol.* **2016**, *17*, 1142−1149.
(33) Wang, C.; Guan, Y.; Lv, M.; Zhang, R.; Guo, Z.; Wei, X.; Du, X.; Yang, J.; Li, T.; Wan, Y.; Su, X.; Huang, X.; Jiang, Z. Manganese Increases the Sensitivity of the cGAS-STING Pathway for Double-Stranded DNA and Is Required for the Host Defense against DNA Viruses. *Immunity* **2018**, *48*, 675.e7.
(34) Sharma, P.; Shin, J. B.; Park, B. C.; Lee, J. W.; Byun, S. W.; Jang, N. Y.; Kim, Y. J.; Kim, Y.; Kim, Y. K.; Cho, N. H. Application of radially grown ZnO nanowires on poly-l-lactide microfibers complexed with a tumor antigen for cancer immunotherapy. *Nanoscale* **2019**, *11*, 4591−4600.
(35) Li, J.; Zheng, P.; Zhao, J.; Chen Peng, R.; Guo, Z. Metal-mediated immune regulations and interventions: prospects of the emerging field of metalloimmunology. *Sci. Sin.: Chim.* **2019**, *49*, 1037−1046.
(36) Wang, C.; Zhang, R.; Wei, X.; Lv, M.; Jiang, Z. Metalloimmunology: The metal ion-controlled immunity. *Adv. Immunol.* **2020**, *145*, 187−241.
(37) Tian, L.; Zhu, Y.; Xu, J.; Shao, M.; Zhu, W.; Xiao, Z.; Chen, Q.; Liu, Z. Coordination Polymers Integrating Metalloimmunology with Immune Modulation to Elicit Robust Cancer Chemoimmunotherapy. *CCS Chem.* **2020**, 2629−2642.
(38) Jin, H.; Qian, Y.; Dai, Y.; Qiao, S.; Huang, C.; Lu, L.; Luo, Q.; Chen, J.; Zhang, Z. Magnetic Enrichment of Dendritic Cell Vaccine in Lymph Node with Fluorescent-Magnetic Nanoparticles Enhanced Cancer Immunotherapy. *Theranostics* **2016**, *6*, 2000−2014.
(39) Cho, N. H.; Cheong, T. C.; Min, J. H.; Wu, J. H.; Lee, S. J.; Kim, D.; Yang, J. S.; Kim, S.; Kim, Y. K.; Seong, S. Y. A multifunctional core-shell nanoparticle for dendritic cell-based cancer immunotherapy. *Nat. Nanotechnol.* **2011**, *6*, 675−682.
(40) Chiang, C. S.; Lin, Y. J.; Lee, R.; Lai, Y. H.; Cheng, H. W.; Hsieh, C. H.; Shyu, W. C.; Chen, S. Y. Combination of fucoidan-based magnetic nanoparticles and immunomodulators enhances

https://doi.org/10.1021/acs.chemmater.1c03681
Chem. Mater. 2021, 33, 9780−9794

tumour-localized immunotherapy. *Nat. Nanotechnol.* **2018**, *13*, 746−754.
(41) Park, J. H.; Geyer, M. B.; Brentjens, R. J. CD19-targeted CAR T-cell therapeutics for hematologic malignancies: interpreting clinical outcomes to date. *Blood* **2016**, *127*, 3312−3320.
(42) Maus, M. V.; Grupp, S. A.; Porter, D. L.; June, C. H. Antibody-modified T cells: CARs take the front seat for hematologic malignancies. *Blood* **2014**, *123*, 2625−2635.
(43) Qian, J.; Zhang, W.; Wei, P.; Yao, G.; Yi, T.; Zhang, H.; Ding, H.; Huang, X.; Wang, M.; Song, Y.; Zhong, S.; Yang, L.; Gao, J.; Zhou, Z.; Wen, L.-p.; Zhang, Y. Enhancing Chemotherapy of p53-Mutated Cancer through Ubiquitination-Dependent Proteasomal Degradation of Mutant p53 Proteins by Engineered ZnFe-4 Nanoparticles. *Adv. Funct. Mater.* **2020**, *30*, No. 2001994.
(44) Pöselt, E.; Kloust, H.; Tromsdorf, U.; Janschel, M.; Hahn, C.; Masslo, C.; Weller, H. Relaxivity Optimization of a PEGylated Iron-Oxide-Based Negative Magnetic Resonance Contrast Agent for T-2-Weighted Spin-Echo Imaging. *ACS Nano* **2012**, *6*, 1619−1624.
(45) Ghosh, D.; Lee, Y.; Thomas, S.; Kohli, A. G.; Yun, D. S.; Belcher, A. M.; Kelly, K. A. M13-templated magnetic nanoparticles for targeted in vivo imaging of prostate cancer. *Nat. Nanotechnol.* **2012**, *7*, 677−682.
(46) Byrne, J. M.; Coker, V. S.; Cespedes, E.; Wincott, P. L.; Vaughan, D. J.; Pattrick, R. A. D.; van der Laan, G.; Arenholz, E.; Tuna, F.; Bencsik, M.; Lloyd, J. R.; Telling, N. D. Biosynthesis of Zinc Substituted Magnetite Nanoparticles with Enhanced Magnetic Properties. *Adv. Funct. Mater.* **2014**, *24*, 2518−2529.
(47) Zhang, Y.; Song, W.; Geng, J.; Chitgupi, U.; Unsal, H.; Federizon, J.; Rzayev, J.; Sukumaran, D. K.; Alexandridis, P.; Lovell, J. F. Therapeutic surfactant-stripped frozen micelles. *Nat. Commun.* **2016**, *7*, No. 11649.
(48) Sun, B.; Chitgupi, U.; Li, C.; Federizon, J.; Zhang, C.; Ruszaj, D. M.; Razi, A.; Ortega, J.; Neelamegham, S.; Zhang, Y.; Lovell, J. F. Drug Delivery: Surfactant-Stripped Cabazitaxel Micelles Stabilized by Clotrimazole or Mifepristone (Adv. Therap. 3/2020). *Adv. Ther.* **2020**, *3*, No. 2070007.
(49) Rennick, J. J.; Johnston, A. P. R.; Parton, R. G. Key principles and methods for studying the endocytosis of biological and nanoparticle therapeutics. *Nat. Nanotechnol.* **2021**, *16*, 266−276.
(50) Resh, M. D. Trafficking and signaling by fatty-acylated and prenylated proteins. *Nat. Chem. Biol.* **2006**, *2*, 584−590.
(51) Missirlis, D.; Khant, H.; Tirrell, M. Mechanisms of Peptide Amphiphile Internalization by SJSA-1 Cells in Vitro. *Biochemistry* **2009**, *48*, 3304−3314.
(52) Vankayala, R.; Huang, Y.-K.; Kalluru, P.; Chiang, C.-S.; Hwang, K. C. First Demonstration of Gold Nanorods-Mediated Photodynamic Therapeutic Destruction of Tumors via Near Infra-Red Light Activation. *Small* **2014**, *10*, 1612−1622.
(53) Sharma, P.; Jang, N.-Y.; Lee, J.-W.; Park, B. C.; Kim, Y. K.; Cho, N.-H. Application of ZnO-based nanocomposites for vaccines and cancer immunotherapy. *Pharmaceutics* **2019**, *11*, No. 493.
(54) Chen, Q.; Sun, L.; Chen, Z. J. Regulation and function of the cGAS−STING pathway of cytosolic DNA sensing. *Nat. Immunol.* **2016**, *17*, 1142−1149.
(55) Wang, C.; Zhang, R.; Wei, X.; Lv, M.; Jiang, Z. Metalloimmunology: The metal ion-controlled immunity. *Adv. Immunol.* **2020**, *145*, 187−241.
(56) Krysko, D. V.; Ravichandran, K. S.; Vandenabeele, P. Macrophages regulate the clearance of living cells by calreticulin. *Nat. Commun.* **2018**, *9*, No. 4644.
(57) Wang, X.; Li, M.; Ren, K.; Xia, C.; Li, J.; Yu, Q.; Qiu, Y.; Lu, Z.; Long, Y.; Zhang, Z.; He, Q. On-Demand Autophagy Cascade Amplification Nanoparticles Precisely Enhanced Oxaliplatin-Induced Cancer Immunotherapy. *Adv. Mater.* **2020**, *32*, No. 2002160.
(58) Raghavan, M.; Wijeyesakere, S. J.; Peters, L. R.; Del Cid, N. Calreticulin in the immune system: ins and outs. *Trends Immunol.* **2013**, *34*, 13−21.
(59) Gardner, A.; Ruffell, B. Dendritic Cells and Cancer Immunity. *Trends Immunol.* **2016**, *37*, 855−865.
(60) Gao, B.; Adhikari, R.; Howarth, M.; Nakamura, K.; Gold, M. C.; Hill, A. B.; Knee, R.; Michalak, M.; Elliott, T. Assembly and antigen-presenting function of MHC class I molecules in cells lacking the ER chaperone calreticulin. *Immunity* **2002**, *16*, 99−109.
(61) Liu, G.; Jiang, Z.; Lovell, J. F.; Zhang, L.; Zhang, Y. Design of a Thiol-Responsive, Traceless Prodrug with Rapid Self-Immolation for Cancer Chemotherapy. *ACS Appl. Bio Mater.* **2021**, *4*, 4982−4989.
(62) Yang, X.; Ren, H.; Zhang, H.; Liu, G.; Jiang, Z.; Qiu, Q.; Yu, C.; Murthy, N.; Zhao, K.; Lovell, J. F.; Zhang, Y. Antibiotic Cross-linked Micelles with Reduced Toxicity for Multidrug-Resistant Bacterial Sepsis Treatment. *ACS Appl. Mater. Interfaces* **2021**, *13*, 9630−9642.

https://doi.org/10.1021/acs.chemmater.1c03681
Chem. Mater. 2021, 33, 9780−9794